

IAEA TECDOC SERIES

IAEA-TECDOC-2026

Intercomparison of k_0 -NAA Software Packages



IAEA

International Atomic Energy Agency

INTERCOMPARISON OF
 k_0 -NAA SOFTWARE PACKAGES

The following States are Members of the International Atomic Energy Agency:

AFGHANISTAN	GEORGIA	PAKISTAN
ALBANIA	GERMANY	PALAU
ALGERIA	GHANA	PANAMA
ANGOLA	GREECE	PAPUA NEW GUINEA
ANTIGUA AND BARBUDA	GRENADA	PARAGUAY
ARGENTINA	GUATEMALA	PERU
ARMENIA	GUYANA	PHILIPPINES
AUSTRALIA	HAITI	POLAND
AUSTRIA	HOLY SEE	PORTUGAL
AZERBAIJAN	HONDURAS	QATAR
BAHAMAS	HUNGARY	REPUBLIC OF MOLDOVA
BAHRAIN	ICELAND	ROMANIA
BANGLADESH	INDIA	RUSSIAN FEDERATION
BARBADOS	INDONESIA	RWANDA
BELARUS	IRAN, ISLAMIC REPUBLIC OF	SAINT KITTS AND NEVIS
BELGIUM	IRAQ	SAINT LUCIA
BELIZE	IRELAND	SAINT VINCENT AND THE GRENADINES
BENIN	ISRAEL	SAMOA
BOLIVIA, PLURINATIONAL STATE OF	ITALY	SAN MARINO
BOSNIA AND HERZEGOVINA	JAMAICA	SAUDI ARABIA
BOTSWANA	JAPAN	SENEGAL
BRAZIL	JORDAN	SERBIA
BRUNEI DARUSSALAM	KAZAKHSTAN	SEYCHELLES
BULGARIA	KENYA	SIERRA LEONE
BURKINA FASO	KOREA, REPUBLIC OF	SINGAPORE
BURUNDI	KUWAIT	SLOVAKIA
CAMBODIA	KYRGYZSTAN	SLOVENIA
CAMEROON	LAO PEOPLE'S DEMOCRATIC REPUBLIC	SOUTH AFRICA
CANADA	LATVIA	SPAIN
CENTRAL AFRICAN REPUBLIC	LEBANON	SRI LANKA
CHAD	LESOTHO	SUDAN
CHILE	LIBERIA	SWEDEN
CHINA	LIBYA	SWITZERLAND
COLOMBIA	LIECHTENSTEIN	SYRIAN ARAB REPUBLIC
COMOROS	LITHUANIA	TAJIKISTAN
CONGO	LUXEMBOURG	THAILAND
COSTA RICA	MADAGASCAR	TOGO
CÔTE D'IVOIRE	MALAWI	TONGA
CROATIA	MALAYSIA	TRINIDAD AND TOBAGO
CUBA	MALI	TUNISIA
CYPRUS	MALTA	TÜRKİYE
CZECH REPUBLIC	MARSHALL ISLANDS	TURKMENISTAN
DEMOCRATIC REPUBLIC OF THE CONGO	MAURITANIA	UGANDA
DENMARK	MAURITIUS	UKRAINE
DJIBOUTI	MEXICO	UNITED ARAB EMIRATES
DOMINICA	MONACO	UNITED KINGDOM OF GREAT BRITAIN AND NORTHERN IRELAND
DOMINICAN REPUBLIC	MONGOLIA	UNITED REPUBLIC OF TANZANIA
ECUADOR	MONTENEGRO	UNITED STATES OF AMERICA
EGYPT	MOROCCO	URUGUAY
EL SALVADOR	MOZAMBIQUE	UZBEKISTAN
ERITREA	MYANMAR	VANUATU
ESTONIA	NAMIBIA	VENEZUELA, BOLIVARIAN REPUBLIC OF
ESWATINI	NEPAL	VIET NAM
ETHIOPIA	NETHERLANDS	YEMEN
FIJI	NEW ZEALAND	ZAMBIA
FINLAND	NICARAGUA	ZIMBABWE
FRANCE	NIGER	
GABON	NIGERIA	
GAMBIA	NORTH MACEDONIA	
	NORWAY	
	OMAN	

The Agency's Statute was approved on 23 October 1956 by the Conference on the Statute of the IAEA held at United Nations Headquarters, New York; it entered into force on 29 July 1957. The Headquarters of the Agency are situated in Vienna. Its principal objective is "to accelerate and enlarge the contribution of atomic energy to peace, health and prosperity throughout the world".

IAEA-TECDOC-2026

INTERCOMPARISON OF
 k_0 -NAA SOFTWARE PACKAGES

INTERNATIONAL ATOMIC ENERGY AGENCY
VIENNA, 2023

COPYRIGHT NOTICE

All IAEA scientific and technical publications are protected by the terms of the Universal Copyright Convention as adopted in 1952 (Berne) and as revised in 1972 (Paris). The copyright has since been extended by the World Intellectual Property Organization (Geneva) to include electronic and virtual intellectual property. Permission to use whole or parts of texts contained in IAEA publications in printed or electronic form must be obtained and is usually subject to royalty agreements. Proposals for non-commercial reproductions and translations are welcomed and considered on a case-by-case basis. Enquiries should be addressed to the IAEA Publishing Section at:

Marketing and Sales Unit, Publishing Section
International Atomic Energy Agency
Vienna International Centre
PO Box 100
1400 Vienna, Austria
fax: +43 1 26007 22529
tel.: +43 1 2600 22417
email: sales.publications@iaea.org
www.iaea.org/publications

For further information on this publication, please contact:

Physics Section
International Atomic Energy Agency
Vienna International Centre
PO Box 100
1400 Vienna, Austria
Email: Official.Mail@iaea.org

© IAEA, 2023
Printed by the IAEA in Austria
July 2023

IAEA Library Cataloguing in Publication Data

Names: International Atomic Energy Agency.
Title: Intercomparison of k_0 -NAA software packages / International Atomic Energy Agency.
Description: Vienna : International Atomic Energy Agency, 2023. | Series: IAEA TECDOC series, ISSN 1011-4289 ; no. 2026 | Includes bibliographical references.
Identifiers: IAEAL 23-01613 | ISBN 978-92-0-139223-7 (paperback : alk. paper) | ISBN 978-92-0-139123-0 (pdf)
Subjects: LCSH: Nuclear activation analysis. | Nuclear activation analysis — Computer software. | Radiochemical analysis. | Nuclear physics.

FOREWORD

Neutron activation analysis (NAA) is an analytical technique implemented in about half the operational facilities worldwide, including most low and medium power research reactors. A precondition for expanding the use of this powerful technique is the demonstration of valid analytical data and organizational quality of the work process. One important aspect of the validity of analytical data is the reported uncertainty, and to estimate that, one needs insight into the uncertainty budget.

The k_0 method for NAA has greatly facilitated the implementation of NAA at new facilities. It allows for the determination of elemental mass fractions, together with their uncertainties, after characterization of the irradiation facility and the detector used, in conjunction with the k_0 database of nuclear data, without the need for sample matched reference materials. As a consequence, software for the application of this method has been developed in several places.

Several of these software packages were demonstrated to function properly by applying them to the analysis of NAA data collected from reference materials. As the mass fractions in reference materials were typically certified with uncertainties of the same order of magnitude as the inherent uncertainties in NAA, the software packages did not seem to contribute significantly to the uncertainty budget. However, as a direct assessment of the accuracy of the codes had not yet been done, and considering that new codes continue to be developed, in 2021 the IAEA organized a comparison of k_0 software packages to determine each software's contribution to the uncertainty budget. Authors of five of the six known k_0 software packages took part in the exercise, including the two widely available codes and three codes developed at particular institutes for their own purposes. This publication presents the results of that comparison.

The IAEA expresses its appreciation to the international experts who contributed to the drafting and review of this publication, in particular M. Blaauw (Netherlands) and R. Jaćimović (Slovenia). The IAEA officer responsible for this publication was N. Pessoa Barradas of the Division of Physical and Chemical Sciences.

EDITORIAL NOTE

This publication has been prepared from the original material as submitted by the contributors and has not been edited by the editorial staff of the IAEA. The views expressed remain the responsibility of the contributors and do not necessarily represent the views of the IAEA or its Member States.

Neither the IAEA nor its Member States assume any responsibility for consequences which may arise from the use of this publication. This publication does not address questions of responsibility, legal or otherwise, for acts or omissions on the part of any person.

The use of particular designations of countries or territories does not imply any judgement by the publisher, the IAEA, as to the legal status of such countries or territories, of their authorities and institutions or of the delimitation of their boundaries.

The mention of names of specific companies or products (whether or not indicated as registered) does not imply any intention to infringe proprietary rights, nor should it be construed as an endorsement or recommendation on the part of the IAEA.

The IAEA has no responsibility for the persistence or accuracy of URLs for external or third party Internet web sites referred to in this publication and does not guarantee that any content on such web sites is, or will remain, accurate or appropriate

CONTENTS

1. INTRODUCTION.....	1
1.1. BACKGROUND.....	1
1.2. OBJECTIVE.....	1
1.3. SCOPE.....	2
1.4. STRUCTURE.....	2
2. BASICS OF THE k_0 -NAA method.....	4
2.1. INTRODUCTION.....	4
2.2. STANDARD k_0 FOR THERMAL AND EPITHERMAL NEUTRON ACTIVATION.....	4
2.2.1. Initial formulation.....	4
2.2.2. Non-ideal epithermal neutron spectrum, self-shielding and true coincidence summing..	5
2.2.3. Additional corrections.....	5
2.2.4. Mass fraction calculation.....	6
2.2.5. Comparator factor.....	7
2.3. FISSION AND THRESHOLD REACTIONS.....	8
2.4. REMAINING CORRECTIONS.....	8
2.5. DETECTOR CHARACTERIZATION.....	8
2.6. IRRADIATION FACILITY CHARACTERIZATION.....	9
3. DESCRIPTION OF THE PARTICIPATING CODES.....	10
3.1. INTRODUCTION.....	10
3.2. HISTORY, INTENDED USE, AND AVAILABILITY.....	10
3.2.1. KayWin.....	10
3.2.2. k0-DALAT.....	10
3.2.3. k0-IAEA.....	10
3.2.4. k0-INRIM.....	10
3.2.5. k0-IPEN.....	11
3.3. GENERAL GAMMA RAY SPECTROMETRY.....	11
3.3.1. KayWin.....	11
3.3.2. k0-DALAT.....	12
3.3.3. k0-IAEA.....	12
3.3.4. k0-INRIM.....	12
3.3.5. k0-IPEN.....	12
3.4. DETECTOR CHARACTERIZATION.....	12
3.4.1. KayWin.....	12
3.4.2. k0-DALAT.....	13
3.4.3. k0-IAEA.....	13
3.4.4. k0-INRIM.....	13
3.4.5. k0-IPEN.....	14
3.5. IRRADIATION FACILITY CHARACTERIZATION.....	14
3.5.1. KayWin.....	14
3.5.2. k0-DALAT.....	15
3.5.3. k0-IAEA.....	15
3.5.4. k0-INRIM.....	16
3.5.5. k0-IPEN.....	16
3.6. ACTIVATION EQUATION CORRECTIONS.....	16
3.6.1. KayWin.....	16
3.6.2. k0-DALAT.....	16
3.6.3. k0-IAEA.....	16
3.6.4. k0-INRIM.....	16

3.6.5. k ₀ -IPEN	17
3.7. INTERPRETATION	17
3.7.1. KayWin	17
3.7.2. k ₀ -DALAT	18
3.7.3. k ₀ -IAEA	18
3.7.4. k ₀ -INRIM	21
3.7.5. k ₀ -IPEN	22
3.8. FEEDBACK TO USER AND REPORTING	22
3.8.1. KayWin	22
3.8.2. k ₀ -DALAT	23
3.8.3. k ₀ -IAEA	23
3.8.4. k ₀ -INRIM	25
3.8.5. k ₀ -IPEN	31
3.9. ADDITIONAL FEATURES	31
3.9.1. KayWin	31
3.9.2. k ₀ -DALAT	32
3.9.3. k ₀ -IAEA	32
3.9.4. k ₀ -INRIM	32
3.9.5. k ₀ -IPEN	32
3.10. OVERVIEW OF FEATURES	32
3.11. ACCEPTED FILE FORMATS	36
4. THE <i>k₀</i> SOFTWARE INTERCOMPARISON.	37
4.1. DATA	37
4.1.1. Data for detector characterization	37
4.1.2. Data for characterization of the irradiation facility	38
4.1.3. Flux monitor and sample spectra	38
4.1.4. Peak areas	40
4.2. INTERCOMPARISON PROCEDURE	40
4.2.1. First round	40
4.2.2. Second round	40
4.2.3. Efficiency curves	41
4.3. RESULTS	42
4.3.1. First round	42
4.3.2. Second round	45
4.3.3. Efficiency curves and true coincidence summing	48
4.3.4. Neutron spectrum parameters	50
4.4. DISCUSSION OF THE RESULTS OBTAINED	51
4.4.1. Mass fractions	51
4.4.2. Neutron spectrum parameters	52
4.4.3. Efficiency curves	55
4.4.4. Gamma ray interferences	55
4.4.5. Threshold reaction interferences	55
5. CONCLUSIONS	56
REFERENCES	59
ABBREVIATIONS	63
CONTENT OF THE ANNEXES	65
CONTRIBUTORS TO DRAFTING AND REVIEW	67

1. INTRODUCTION

1.1. BACKGROUND

Neutron activation analysis (NAA) is a method to determine mass fractions of the chemical elements by inducing radioactivity through neutron irradiation and detecting emitted radiation. If no chemical separations are applied and delayed gamma rays are detected with germanium detectors, the technique has been historically named instrumental neutron activation analysis (INAA), a term still often used in the NAA community.

To obtain quantitative results, the method needs standardization. The most accurate approach is to co-irradiate a standard material, containing a known amount of the element, with the unknown sample and measure both using the same detector arrangement. Because multi-element standards are hard to make, single-comparator methods were developed where the “sensitivity” for all elements is related to a single element of choice. After co-irradiating standards of each element with the comparator element, and measuring them in the same detector arrangement to determine the relative sensitivity, only standards of the single comparator element need be co-irradiated and measured with the unknown sample.

More flexibility can be obtained when the detector efficiency is determined separately, for all counting geometries used. The resulting relative sensitivities are now named “k factors” and can be identified as compound nuclear constants, that need be determined only once for each irradiation facility used. Even more flexibility is achieved by modelling the neutron spectrum in the irradiation facilities, allowing for characterization through the determination of just a few parameters. The dependence of the ‘k factors’ on these same neutron spectrum parameters is also established. The ‘k factor’, at this stage, was named the ‘ k_0 factor’. Originally presented in 1975 [1], the associated k_0 -NAA method quickly established itself all over the world as the easiest way to get good results from INAA analyses.

The k_0 -NAA method was developed with a software suite by the originators of the method. Specific codes were written to characterize the detector, convert efficiency curves from the ‘reference geometry’ to others (SOLANGE by Moens [2]), to calculate true coincidence-summing corrections (SOLCOI by De Wispelaere), and others. The software ran on VAX-VMS computers.

Later on, the original software was ported to the IBM-PC by R. van Sluijs and offered as a commercial product with great success [3–5]. This software package is now known as KayWin. The IAEA, in its efforts to enhance the utilization of research reactors, engaged M. Blaauw and M. Bacchi to develop a similar package named k_0 -IAEA, and made it available for free [6, 7]. In-house software was also developed in Brazil by M. Da Silva Dias and R. Semmler, in China by the Chinese Institute of Atomic Energy, in Italy by G. D’Agostino and M. Di Luzio (k_0 -INRIM, [8, 9]), and in Viet Nam, by Ho Manh Dung. Other k_0 -related approaches were implemented in Portugal by C. Freitas, in München by Z. Revay (for prompt gamma activation analysis specifically) and in Canada by G. Kennedy.

1.2. OBJECTIVE

All these codes for k_0 -NAA slightly differ from each other in the way they work — detector efficiencies are modelled and converted in different ways, corrections are taken into account or not, and mass fractions obtained from single gamma ray peaks are combined into final results by different strategies. The IAEA therefore saw a need to establish the magnitude of the impact on the final mass fractions determined by the different software packages.

A number of papers have been published on the estimation of the combined standard uncertainty in mass fractions as obtained with the k_0 -NAA method (e.g. Ref. [10]). The stated uncertainties in the k_0 factors, which are typically around 1%, have been shown to be a minor part of the overall uncertainties, which are typically around 3.5%. Propagation of uncertainties considering all contributions to the uncertainty is a challenging task due to strong correlations between the nuclear data (i.e. half-life, Q_0 value, effective resonance energy) and the k_0 factors, a strong correlation between the neutron spectrum parameters f and α , and also due to strong correlations between the mass fractions obtained using different gamma ray energies or different measurements (short, medium, long) of the same sample. The main independent source of uncertainty for individual mass fractions to be considered is the uncertainty in the peak areas due to counting statistics. This makes it relatively easy to propagate, and sometimes it is the only source of uncertainty that is taken into account. Other sources of uncertainty that affect all mass fractions, such as the mass of the flux monitor or the irradiation duration, are also easy to propagate.

1.3. SCOPE

The IAEA has previously conducted intercomparison exercises for gamma ray spectrometry [11–13], alpha spectrometry [14–17], particle induced X ray emission (PIXE) codes [18, 19], particle induced gamma ray emission (PIGE) software packages [20] and ion-beam analysis (IBA) techniques including Rutherford backscattering (RBS), elastic-recoil detection analysis (ERDA) and nuclear reaction analysis (NRA) software packages [21]. One of the main conclusions of these intercomparison exercises was that, in general, the codes were appropriate for their stated purpose, while nevertheless significant differences between codes were found in some cases. It is clear that the influence of using different software packages on the results obtained needs to be ascertained and quantified, in order to provide assurance that the software package used does not significantly affect the final uncertainty.

For NAA, a limited intercomparison was done for two k_0 -NAA codes [22]. One main conclusion of Ref. [22] was that “in general, a good agreement was found between the elements contents determined by both codes and certified, non-certified and/or assigned values” of the certified reference materials (CRM) analysed. However, the intercomparison was not made by the authors of the codes, and therefore there was no guarantee that the codes were used as well as they could be. It should also be considered that other k_0 -NAA codes also exist or have been developed since the intercomparison. Therefore, it was decided to perform the current intercomparison.

A call for participation in the intercomparison was issued by the IAEA through the k_0 International Scientific Committee, and subsequently all known k_0 -NAA codes were invited to participate. Five out of six codes identified accepted to participate in the exercise.

1.4. STRUCTURE

Following this introduction, Section 2 describes the basics of the k_0 -NAA method, in order to provide the vocabulary needed to clarify the differences in implementation between the participant codes. In Section 3 the codes themselves are presented, and details of their features are provided. Section 4 describes the intercomparison exercise, including the data made available to the participants, the intercomparison procedure, the results obtained and their analysis. Section 5 presents the conclusions of the intercomparison, and provides best practices for the practice of k_0 -NAA method.

In addition, several Annexes are made available in electronic form, allowing interested readers to reproduce the calculations, as well as to use the data to test future newly developed code, namely the intercomparison dataset, the template for reporting on all results and the results as reported by the participants, in Annexes 1, 2 and 3, respectively.

2. BASICS OF THE k_0 -NAA METHOD

2.1. INTRODUCTION

In its original version, the k_0 -method for INAA was applicable only to '1/v' (n, γ)-reactions, i.e. reactions where the capture cross section is inversely proportional to the neutron velocity. Various corrections were introduced with time, such as the Westcott factor $g(T)$, that accounts for the non-1/v behaviour of neutron capture.

2.2. STANDARD k_0 FOR THERMAL AND EPITHERMAL NEUTRON ACTIVATION

2.2.1. Initial formulation

In the first sets of expressions used by Simonits et al. [1], the linear relation between the count rate in a specific gamma ray peak and the amount of element present in the sample was expressed with

$$N_p/t_m = w \left(\frac{\gamma \theta N_{av}}{M} \right) (\Phi_s \sigma_0 + \Phi_{epi} I_0) S D C \varepsilon \quad (1)$$

where

- N_p is the peak area,
- t_m the measurement time (s),
- w the amount of element (g),
- γ the gamma ray yield,
- θ the isotopic abundance,
- N_{av} Avogadro's number,
- M the atomic mass (g),
- Φ_s the subcadmium (a.k.a. thermal) neutron fluence rate ($m^{-2}s^{-1}$),
- σ_0 the thermal capture cross section (m^2),
- Φ_{epi} the epicadmium (a.k.a. epithermal) neutron fluence rate ($m^{-2}s^{-1}$),
- I_0 the resonance integral (m^2)
- S the saturation factor ($1 - e^{-\lambda \cdot t_{irr}}$),
- D the decay factor ($e^{-\lambda_d \cdot t}$),
- C the counting factor ($(1 - e^{-\lambda \cdot t_m}) / (\lambda \cdot t_m)$), and
- ε the detection efficiency.

Here, the saturation factor S is defined as

$$S = 1 - e^{-\lambda t_{irr}} \quad (2)$$

where λ is the decay constant (s^{-1}) and t_{irr} is the irradiation time (s).

The decay factor D is defined by

$$D = e^{-\lambda t_d} \quad (3)$$

where t_d is the decay time between irradiation time and measurement (s).

The counting factor C is defined by

$$C = \frac{(1 - e^{-\lambda t_m})}{\lambda t_m} \quad (4)$$

where t_m is the duration of the measurement (s).

S, D and C can get more complicated if the radionuclide measured in the end is not exclusively and directly produced by a single (n, γ)-reaction.

With the definition of $Q_0 = I_0/\sigma_0$, the main expression becomes

$$N_p/t_m = w \left(\frac{\gamma \theta N_{av}}{M} \right) \sigma_0 (\Phi_s + \Phi_{epi} Q_0) SDC \varepsilon \quad (5)$$

2.2.2. Non-ideal epithermal neutron spectrum, self-shielding and true coincidence summing

A correction for a non-ideal epithermal neutron spectrum shape was introduced with the α -parameter to characterize the deviation, and the effective resonance energy E_r to reflect the reaction's sensitivity to α . The resonance integral I_0 as well as Q_0 became a function of α . The dependence of $Q_0(\alpha)$ on α and the effective resonance energy E_r is given by

$$Q_0(\alpha) = \frac{Q_0(0) - 0.429}{E_r^\alpha} + \frac{0.429}{(2\alpha + 1)E_{Cd}^\alpha} \quad (6)$$

where

E_{Cd} is the Cd-cutoff energy (0.55 eV), and

E_r is the effective resonance energy (eV).

Also, correction factors g_{th} and g_{epi} were introduced for thermal and epithermal neutron self-shielding during irradiation, and a factor c for true coincidence summing during measurement. The detector efficiency ε is understood to cover differences in counting geometry due to sample distance, sample shape and gamma ray self-absorption. With all that, the main expression becomes

$$N_p/t_m = w \left(\frac{\gamma \theta N_{av}}{M} \right) \left(g_{th} \Phi_s \sigma_0 + g_{epi} \Phi_{epi} I_0(\alpha) \right) SDC c \varepsilon \quad (7)$$

where

$I_0(\alpha)$ is the α -dependent resonance integral (m^2),

α the parameter that accounts for non-ideal 1/E epithermal flux distributions,

g_{th} the thermal self-shielding factor,

g_{epi} the epithermal self-shielding factor, and

c coincidence correction factor.

2.2.3. Additional corrections

After De Corte published his milestone habilitation thesis [23], work was done to incorporate corrections for non-1/v reactions using the Westcott factor $g(T)$. The k_0 community never came to a unified expression for this – the following is the implementation in the k0-IAEA software.

$$N_p/t_m = w \left(\frac{\gamma \theta N_{av}}{M} \right) \left(g_{th} \Phi_s g(T) \sigma_0 + g_{epi} \Phi_{epi} I_0(\alpha) \right) \quad (8)$$

where $g(T)$ is the Westcott factor (and T the Maxwell/Boltzmann neutron temperature of the thermal part of the neutron velocity distribution).

With the definition of the thermal/epithermal ratio $f = \Phi_s/\Phi_{epi}$, the main expression becomes

$$N_p/t_m = SDCw \left(\frac{\gamma\theta N_{av}}{M} \right) \Phi_s \sigma_0 \left(g_{th}g(T) + g_{epi} \frac{Q_0(\alpha)}{f} \right) c\varepsilon \quad (9)$$

The mass of the element w is separated into sample mass m and element mass fraction ρ , where $w = \rho m$, to get

$$\frac{N_p/t_m}{SDC} = w \left(\frac{\gamma\theta N_{av}}{M} \right) \Phi_s \sigma_0 \left(g_{th}g(T) + g_{epi} \frac{Q_0(\alpha)}{f} \right) c\varepsilon \quad (10)$$

For legibility, a ‘‘specific count rate’’ A_{sp} (in $s^{-1} g^{-1}$), that expresses the sensitivity for the element of interest, is defined by

$$A_{sp} = \frac{N_p/t_m}{SDCw} \quad (11)$$

which, with

$$\frac{N_p/t_m}{SDCw} = \left(\frac{\gamma\theta N_{av}}{M} \right) \Phi_s \sigma_0 \left(g_{th}g(T) + g_{epi} \frac{Q_0(\alpha)}{f} \right) c\varepsilon \quad (12)$$

leads to

$$A_{sp} = \left(\frac{\gamma\theta N_{av}}{M} \right) \Phi_s \sigma_0 \left(g_{th}g(T) + g_{epi} \frac{Q_0(\alpha)}{f} \right) c\varepsilon \quad (13)$$

2.2.4. Mass fraction calculation

Mass fractions ρ and sample mass m are defined, where the previously defined w satisfies $w = \rho m$, and indices a and c are attached for analyte and comparator, respectively, on order to arrive at the expression that is to be used to calculate a mass fraction ρ_a .

$$\frac{\frac{N_{p,a}/t_{m,a}}{(SDC)_a}}{\frac{N_{p,c}/t_{m,c}}{(SDC)_c}} = \frac{\rho_a m_a \left(\frac{\gamma_a \theta_a N_{av}}{M_a} \right) \Phi_{s,a} \sigma_{0,a} \left(g_{th,a} g_a(T) + g_{epi,a} \frac{Q_{0,a}(\alpha)}{f} \right) c_a \varepsilon_a}{\rho_c m_c \left(\frac{\gamma_c \theta_c N_{av}}{M_c} \right) \Phi_{s,c} \sigma_{0,c} \left(g_{th,c} g_c(T) + g_{epi,c} \frac{Q_{0,c}(\alpha)}{f} \right) c_c \varepsilon_c} \quad (14)$$

Legibility improvement again by using A_{sp}

$$\frac{A_{sp,a}}{A_{sp,c}} = \frac{\rho_a \left(\frac{\gamma_a \theta_a N_{av}}{M_a} \right) \Phi_{s,a} \sigma_{0,a} \left(g_{th,a} g_a(T) + g_{epi,a} \frac{Q_{0,a}(\alpha)}{f} \right) c_a \varepsilon_a}{\rho_c \left(\frac{\gamma_c \theta_c N_{av}}{M_c} \right) \Phi_{s,c} \sigma_{0,c} \left(g_{th,c} g_c(T) + g_{epi,c} \frac{Q_{0,c}(\alpha)}{f} \right) c_c \varepsilon_c} \quad (15)$$

and solving for ρ_a

$$\rho_a = \rho_c \frac{A_{sp,a}}{A_{sp,c}} \frac{\left(\frac{\sigma_{0,c} \gamma_c \theta_c}{M_c} \right)}{\left(\frac{\sigma_{0,a} \gamma_a \theta_a}{M_a} \right)} \frac{c_c \varepsilon_c}{c_a \varepsilon_a} \frac{\Phi_{s,c} \left(g_{th,c} g_c(T) + g_{epi,c} \frac{Q_{0,c}(\alpha)}{f} \right)}{\Phi_{s,a} \left(g_{th,a} g_a(T) + g_{epi,a} \frac{Q_{0,a}(\alpha)}{f} \right)} \quad (16)$$

With the definition of the k_0

$$k_{0,a} = \left(\frac{\sigma_{0,a} \gamma_a \theta_a}{M_a} \right) / \left(\frac{\sigma_{0,Au} \gamma_{Au} \theta_{Au}}{M_{Au}} \right) \quad (17)$$

the final expression is obtained:

$$\rho_a = \rho_c \frac{A_{sp,a}}{A_{sp,c}} \frac{k_{0,c}}{k_{0,a}} \frac{c_c \varepsilon_c}{c_a \varepsilon_a} \frac{\Phi_{s,c} (f g_{th,c} g_c(T) + g_{epi,c} Q_{0,c}(\alpha))}{\Phi_{s,a} (f g_{th,a} g_a(T) + g_{epi,a} Q_{0,a}(\alpha))} \quad (18)$$

2.2.5. Comparator factor

Since the equation above is to be used over and over again for the single comparator to calculate a number of analyte mass fractions, it makes sense to define a comparator factor F_c (in $\text{g}^{-1}\text{s}^{-1}$) with

$$\frac{1}{F_c} = \frac{\rho_c}{A_{sp,c}} \frac{k_{0,c}}{1} c_c \varepsilon_c \left(f g_{th,c} g_c(T) + g_{epi,c} Q_{0,c}(\alpha) \right) \quad (19)$$

so that analyte mass fractions can be calculated with

$$\rho_a = \frac{A_{sp,a}}{F_c} \frac{1}{k_{0,a}} \frac{1}{c_a \varepsilon_a} \frac{\Phi_{s,c}}{\Phi_{s,a}} \frac{1}{\left(f g_{th,a} g_a(T) + g_{epi,a} Q_{0,a}(\alpha) \right)} \quad (20)$$

To compute $\Phi_{s,c}$ from F_c , the equation above can be rewritten as

$$\frac{A_{sp,c}}{\rho_c} = F_c \frac{k_{0,c}}{1} c_c \varepsilon_c \left(f g_{th,c} g_c(T) + g_{epi,c} Q_{0,c}(\alpha) \right) \quad (21)$$

and compared to

$$\frac{N_p/t_m}{SDCW} = \left(\frac{\gamma \theta N_{av}}{M} \right) \frac{\Phi_s \sigma_0}{f} c \varepsilon \left(f g_{th} g(T) + g_{epi} Q_0(\alpha) \right) \quad (22)$$

so that, with $k_{0,c} = 1$ in the specific case of gold as comparator element,

$$F_c = \left(\frac{\gamma \theta N_{av}}{M} \right) \frac{\Phi_s \sigma_0}{f} \quad (23)$$

or, with $\gamma = 0.955$, $\theta = 1$, $N_{av} = 6.023 \times 10^{23} \text{ mol}^{-1}$, $M = 196.97 \text{ g mol}^{-1}$ and $\sigma_0 = 98.7 \times 10^{-28} \text{ m}^2$ becomes

$$F_c = \frac{\Phi_s}{f} / 3.47 * 10^4 \quad (24)$$

or, if fluxes and cross sections are expressed in $\text{cm}^{-2}\text{s}^{-1}$ and cm^2 , and the mass fraction is to come up in mg/kg , as stated in the 'KayWin Vademecum' [24]:

$$F_c = \frac{\Phi_s}{f} / 3.47 * 10^6 \quad (25)$$

2.3. FISSION AND THRESHOLD REACTIONS

Early on, fission reactions were not considered in the k_0 -NAA method. Since ^{235}U fission is a mostly thermal neutron capture reaction that yields readily detectable radionuclides, it was easily included with the existing set of equations and corrections.

Threshold reactions due to capture of high-energy neutrons are not considered in the k_0 -NAA method at the time of writing (2022). At the same time, some of the software packages for k_0 -NAA do account for them, using

$$N_p/t_m = w \left(\frac{\gamma \theta N_{av}}{M} \right) (\Phi_f \sigma_f) SDC \varepsilon \quad (26)$$

where

Φ_f is the fast neutron flux ($\text{m}^{-2}\text{s}^{-1}$), and
 σ_f the threshold capture cross section (m^2),

One might say that the neutron spectrum is characterized with a fifth parameter (Φ_s, f, α, T and Φ_f), same as the reaction ($\sigma_0, Q_0, E_r, g(T)$ and σ_f). For any given reaction, however, either σ_0 or σ_f is 0.

2.4. REMAINING CORRECTIONS

Under extreme conditions, such as very high neutron fluence rates and/or very long irradiation times, even the simplest activation process is complicated by the number of target atoms decreasing significantly during activation. This phenomenon is called ‘burnup’.

Another phenomenon is the capture of neutrons by a reaction product. This may produce yet another detectable radionuclide (secondary activation), and it may also result in a significant loss of the first reaction product (secondary burnup).

The severity of all these phenomena depends on the product of neutron fluence rate, capture cross section and irradiation duration. None of these are considered in the ‘official’ k_0 -NAA method, where they are considered to be negligible, but some software packages do take them into account.

2.5. DETECTOR CHARACTERIZATION

The detector’s *relative* full energy peak efficiency curve, defining the probability of detecting all of a gamma ray’s energy, must be determined as a function of gamma ray energy in order to use the k_0 -NAA method. Since comparator and sample are to be measured on the same detector and the ratio of detection efficiencies appears in the mass fraction calculation equation, it does not matter if the curve is off in its entirety by some factor, as long as the shape is correct.

The original set of k_0 factors was determined through measurements at large distances from the detectors, to avoid true coincidence summing. The efficiency of these detectors was modelled using a linear relation on a log-log scale at higher energies. At lower energies, polynomials of different orders were used in different energy regions. This implies that in order to obtain maximum accuracy with the k_0 -NAA method, the same efficiency curve model as the one used for determination of the k_0 factors is necessary. On the other hand, using better models requiring fewer data points to establish the curve is convenient. The various participant codes offer different approaches to this.

Often, to achieve the lowest detection limits, samples are counted close to the detector, not necessarily at the same distance as the comparator. To accommodate this, the k_0 founders developed the SOLANGE [2] software to convert detector efficiencies from the ‘reference’ geometry to closer geometries. To this end, numerical integration was performed over sample and detector volume, taking gamma ray absorption in the sample as well as in intermediate layers into account. The participant codes all address this issue in a different manner.

When measuring close to the detector, multiple photons emitted simultaneously by the same atom can be detected as one. The phenomenon is named ‘true coincidence summing’. If photons are completely detected, ‘summing in’ results in increased peak areas at the total of the summed energies, or even to artificial ‘sum’ peaks that do not correspond to a single energy emitted by the atom. If some of the photons are not completely detected, ‘summing out’ will result in decreased peak areas. Calculating the corrections for this involves an additional efficiency curve named the ‘peak-to-total’ curve. Also, the full energy peak efficiency curve must be *absolute* for correct true coincidence calculations (as opposed to a *relative* curve that could be determined using a radioactive source of unknown magnitude, emitting multiple gamma rays). The participant codes all deal with this in their own way.

2.6. IRRADIATION FACILITY CHARACTERIZATION

The irradiation facility must be characterized in terms of neutron spectrum parameters Φ_s, f, α, T and Φ_f . To this end, flux monitors consisting of elements that exhibit different Q_0 and E_r -values must be irradiated together and measured. If the fast flux is to be assessed, a suitable element must be added for that. One strategy is to stack foils of a few materials and irradiated them as such, called the ‘bare monitor’ method. Typical combinations used for this are Al-Au alloy and Zr. The $^{27}\text{Al}(n,p)^{27}\text{Mg}$ reaction represents the fast flux, and $^{197}\text{Au}(n,\gamma)^{198}\text{Au}$, $^{94}\text{Zr}(n,\gamma)^{95}\text{Zr}$ and $^{96}\text{Zr}(n,\gamma)^{97}\text{Zr}$. Fe could be added to use the $^{54}\text{Fe}(n,p)^{54}\text{Mn}$ reaction for the fast flux, or Ni to use the $^{58}\text{Ni}(n,p)^{58}\text{Co}$. An alternative for Au plus Zr is the combination of Cr, Mo and Au. Instead of stacking metal foils, one can also choose to dissolve the compounds and pipet known amounts on filter paper in capsules.

The temperature is often estimated as the temperature of the cooling water in the reactor, typically 300 K. If it is to be assessed experimentally, Lu is the element of choice to use, with $g(T)$ values that strongly depend on T .

To separate subcadmium and epicadmium neutron fluence rates, irradiations with and without 1 mm thick Cd-cover can be applied — the Cd layer stops 99% of the subcadmium neutrons from reaching the monitor foils. The different participant codes offer various options in this respect.

When irradiating samples, these are often sandwiched between flux monitors to allow for interpolation, since gradients can occur for each neutron spectrum parameter. A gradient might also be established at initial characterization time, and used later on. The different participant codes also offer various options in this respect.

3. DESCRIPTION OF THE PARTICIPATING CODES

3.1. INTRODUCTION

The k_0 -NAA method only establishes the proportionality between a specific, dead-time corrected gamma ray peak area and the mass fraction of the associated chemical element. It does not specify how to determine a peak area. It exclusively applies to selected gamma rays with non-zero gamma ray yields, i.e. not to single or double escape peaks, nor to pure sum peaks. It exclusively applies to thermal (n,γ) and thermal fission activation reactions. In order to produce an analysis result, much more must be done. In this chapter, a description of the participant codes is offered with respect to k_0 -NAA method features as well as of other features offered.

3.2. HISTORY, INTENDED USE, AND AVAILABILITY

In this section the history, intended use, and availability of each participating code is briefly discussed.

3.2.1. KayWin

Kayzero for Windows (a.k.a. ‘KayWin’ V3.37) is the successor of Kayzero, the DOS-based software developed at DSM Research in the Netherlands for its in-house NAA. Apart from thermal INAA, the code was developed with epithermal INAA in mind, as well as low-energy photon detectors. The software is commercially available from ‘k0-ware’, Heerlen, The Netherlands.

3.2.2. k0-DALAT

The k0-DALAT (2019 version) code can automatically process gamma ray spectrum, calculate the detector efficiency, calculate neutron flux parameters and calculate the mass fraction, uncertainty and detection limit of the element of interest. It is applicable to thermal and epithermal INAA. The software is in use at the Dalat research reactor in Viet Nam.

3.2.3. k0-IAEA

The k0-IAEA code was developed at the IAEA’s request in the early 2000s, by M. Blaauw, M. Bacchi, M. Rossbach and Lin Xilei. The first version implemented the k_0 -NAA method as specified in De Corte’s aggregate thesis [23]. It did not include peak area determination, but it accommodated a large set of input file formats. Over the years, peak area determination was included, epithermal self-shielding using Trkov’s MATSSF [25, 26] approach, prompt gamma spectrum interpretation, and quality assurance and quality control (QA/QC) features for follow up of reference material and blank results. The code was not developed with epithermal NAA in mind, but can still be used to that end. The same goes for low-energy photon detectors. The software has always been available for free through the IAEA [27]. The current version is 9.10 (2021).

3.2.4. k0-INRIM

The k0-INRIM code (version 2.0, 2021) is developed and used at the Italian National Institute of Metrological Research (INRIM) [8, 9]. It is a freely distributed open source project written in python3 programming language that was conceived to assist NAA analysts during data elaboration and uncertainty evaluation following the recommendations of the guide to the

expression of uncertainty in measurement (GUM) [28]. The main aim was to make automatic the compiling of the uncertainty spreadsheets [29] for the k_0 standardisation analysis, thus reports are obtained in Microsoft Excel format.

Many efforts have been made to implement a measurement equation modelling the experimental input data in fine details. This required the adoption of an original approach for the detector efficiency characterisation based on a fully experimental procedure without the need for Monte Carlo simulations.

The user interface of the software was designed to be friendly, schematic and intuitive. Built-in functions for the automatic determination of (i) monitor to analyte efficiency ratio, (ii) neutron flux parameters by ‘triple bare method’, (iii) neutron flux gradient at the irradiation channel and (iv) peak-to-total ratios were implemented. A number of corrections are evaluated and applied, e.g. (i) sample positioning misplacements, (ii) extended sample geometry, (iii) gamma self-absorption, (iv) true-coincidence, (v) counting pile-up, (vi) blank and (vii) moisture. In addition, there are features implemented to (i) identify peaks from gamma spectra for easy recognition of target elements and (ii) recall and re-analyse the data starting from gamma spectra to output the result with the uncertainty budget for quality assurance requirements.

The software does not provide peak area determination but accepts peak elaboration and spectra information input from GammaVision [30] and/or HyperLab [31] outputs. The equation model [32] implemented in the present version is based on the Hogdahl convention and applies to activation and decay path types I, IIB, IVB and VI defined in Ref. [23] as well as to $1/\nu$ nuclides; if those conditions are not met, warnings are issued.

It is worth to note that the use of the current version allows performing analysis that feature experimental setups concerning sample (containing the investigated elements) and standard (containing the monitor element) gamma acquisitions in different counting positions, albeit at least one of the two should be in the reference position; moreover, extended geometry of samples and standards are taken into account.

3.2.5. k0-IPEN

The k0-IPEN code (version 1.7, 2021) was developed and is in use at IPEN, Brazil.

3.3. GENERAL GAMMA RAY SPECTROMETRY

General software for gamma-ray spectrometry is also used for radionuclide activity measurements, so some of the k_0 -NAA method software developers chose to use the output of such software, in terms of peak areas and energies, as input for their own k_0 software, instead of programming their own peak fitting algorithms. Some codes offer both: importing peak areas determined externally, or determining them internally. The latter capability was not used in the current intercomparison. Such peak areas must be corrected for dead time as well as for background before they can be considered to be proportional to the element’s mass fraction. Most participant codes offer that capability.

3.3.1. KayWin

The code relies on external peak-fitting codes, but has options for energy calibration and correct fake peaks that are added to improve peak fitting of broad peaks. It can also use correctly dual

mode LFC spectra and a dead-time stabilizer. Plans exist to incorporate the Deimos code [33] in the near future.

3.3.2. k0-DALAT

The code is capable of automatic gamma-ray spectrum processing, determining peak areas and energies.

3.3.3. k0-IAEA

The k0-IAEA code includes peak-area determination capabilities. Peak-shape calibration, energy calibration and interactive multiplet fitting are included. Dead-time correction can be based on live time/real time data in the spectrum file, or on the measured area of a pulser peak, if present in the spectrum.

A special property of the code is that it will allow for negative peak areas as the outcome of the fitting process. This may seem counterintuitive, but forcing positive outcome will bias results, in a manner that becomes noticeable if repeated measurements are performed of a mass fraction that is well below the detection limit.

3.3.4. k0-INRIM

The code relies on external peak-fitting codes. It recalls spectra information from a combination of two files: the so-called peak list (the list of all identified peaks in the investigated spectrum including centroid channel, energy and peak area) and the spectrum itself (the list of counts for any channel including acquisition times). Peak lists are recalled through either GammaVision report output (.rpt format) or HyperLab output (.csv format) while spectrum information are recalled through either GammaVision spectrum file (.chn format) or HyperLab ASCII converted spectrum (.asc format). In case the .rpt GammaVision file is recalled as peak list, spectrum data are optional, they are mandatory otherwise.

3.3.5. k0-IPEN

Routine Alpino, imbedded in the k0-IPEN package, can calculate peak areas for well separated peaks. For overlapped peaks, the code relies on external peak-fitting codes. It can read peak list files from Hypermet or HyperLab codes in ASCII format.

3.4. DETECTOR CHARACTERIZATION

General software for gamma-ray spectrometry can be used to determine efficiency curves (both full energy and peak-to-total, these days), but all participant codes implemented that internally. Conversion of one geometry-specific detector efficiency to another is performed internally by some, but not by all participant codes. And when they do it internally, they use different methods.

3.4.1. KayWin

The conversion of efficiency from one geometry (counting vial or source geometry and position) to a different one is done using effective solid angles calculated using SOLANGE [2] and coincidence correction factors calculated using COINCALC [34]. Both calculations are based on the original codes from Frans De Corte, Andras Simonits, Antoine De Wispelaere and Luc Moens.

In particular, KayWin still uses the process from those codes, which are based on fits of the reference efficiency with second or third order polynomials using three or four regions of interest. The reference full energy peak efficiency was determined using data from all the measurements of calibration standards that were provided for the intercomparison. Fine tuning of the dead layer thickness and vacuum gap can be performed automatically using true coincidence-free sources if needed.

For the peak-to-total efficiency curve, multiple mono-energetic spectra are used.

3.4.2. k0-DALAT

A fourth-order polynomial is used to determine the full energy peak detector efficiency. To convert the efficiency from one geometry to other counting geometries, the Angle code (Version 3) [35] is used. It converts the reference efficiency to the actual counting geometries. The TrueCoinc code [36] is used to calculate true coincidence summing correction factors.

3.4.3. k0-IAEA

The code assumes that the peak-to-total curve can be approximated by a straight horizontal line at unity value up to 200 keV, followed by a sloped straight line on a log-log scale. This means that the curve can be determined from only one data point, obtained from a ^{137}Cs or some such nuclide that emits only a single gamma ray. Alternatively, multiple data points can be imported from a text file, and fitted. The peak-to-total curve is considered to be applicable to all counting geometries.

The full energy peak efficiency curve consists of a sixth-order polynomial with related parameters, ending up with four degrees of freedom [37]. The curve can be fitted to any single spectrum with suitable peaks, acquired in any counting geometry, and true coincidence summing effects are taken into account in the process. So, a standard calibration source with ^{109}Cd , ^{137}Cs , ^{65}Zn , ^{60}Co and ^{88}Y can be employed at a large distance from the detector, but also right on the endcap or inside a well-type detector. ^{152}Eu , with its X-rays near 40 keV, can be used as a single nuclide to determine the whole curve. Extrapolation to higher energies is quite reliable, but gets better when the calibration source yields higher-energy gamma rays.

The code converts the full energy efficiency curve from one counting geometry to the other using embedded Monte Carlo methods with a user-defined statistical precision — typically 0.1%. Sample composition and dimensions are taken into account fully, same as detector dimensions and intermediate layers. Simulations are performed for a predefined set of energies, and the polynomial is fitted to the results afterwards. Gamma ray self-absorption in the sample is accounted for in the process, but not available as a separate correction factor number.

3.4.4. k0-INRIM

The software relies on a fully experimental detector characterization, completely internally performed, to compute full energy-peak efficiency curves. Calibrated gamma sources are acquired at all counting positions that are to be characterized. The farthest counting position is labelled as reference and an exponential 6-terms polynomial full energy efficiency curve is fitted on it; at the other counting positions only coincidence-free emissions are considered to calculate count rate ratios with respect to reference, afterwards, polynomial curves are fitted to the count rate ratios data.

The software uses the full energy peak efficiency curve at reference to evaluate efficiencies at reference position while polynomial curves from count rate ratios are used to convert efficiencies from reference to other counting positions [38].

The peak-to-total curves are obtained using spectra of mono-energetic sources. Peak-to-total fits are performed using two functions (a two term polynomial and a straight line) joined at the energy E_j defined by the user; conditions to ensure a smooth junction are enforced such as the equality of y points and first derivatives at E_j .

Geometry corrections are also calculated from the information gathered during the detector characterization; they are based on the assumptions that the quadratic attenuation of efficiency versus distance holds locally and on the condition of cylindrical shaped samples placed along the axis of the detector end-cap. For each counting position, local point of action distances within the detector, d_0' , for any coincidence-free emission counted during detector characterization are evaluated by means of two term polynomial functions. An exponential 5-terms polynomial function is fitted to d_0' points for any counting position to evaluate the geometry correction together with the height of the sample.

Self-absorption corrections are applied based on physical sample characteristics (sample height and composition) and literature data [39].

Outputs of the detector characterizations are saved on disc and can be easily recalled, if needed.

3.4.5. k0-IPEN

The software incorporates routines to calculate the experimental peak efficiencies and P/T ratios for the standard sources, together with all the corresponding uncertainties; to correct the peak efficiencies for coincidence summing; to fit the peak efficiencies and P/T ratios with log-log polynomial functions. A fourth-order polynomial is fitted to the available data at the reference position. For the actual counting geometries, the efficiencies are determined by Monte Carlo calculations using MCNP6 [40] and verified using spectra measured at those distances.

3.5. IRRADIATION FACILITY CHARACTERIZATION

The characterization of the irradiation facility in terms of neutron spectrum parameters is quite specific for neutron activation analysis. Each participant code offers options for that purpose. The methods employed by the different codes are not identical, and therefore it is expected that they will lead to different spectrum parameters, which in turn will influence the calculated mass fractions.

3.5.1. KayWin

For neutron spectrum calibration, the 'multi monitor bare', 'Cd-cover' and 'Cd-ratio' methods are implemented, as well as the 'triple bare' and the 'special Au-Zr triple bare' methods, as described in the Vademecum [24]. The result of the measurement of a comparator is contained in the comparator factor F_c (see section 2.2.1). The comparator can be seen as a flux monitor. In case of a non-uniform flux distribution across the sample container, the F_c factor can be used to determine the flux at the sample's location.

3.5.2. k0-DALAT

To determine the neutron spectrum parameters, the ‘triple bare’ or ‘triple Cd-covered’ methods are applied for thermal and epithermal INAA, respectively, using Al-Au plus Zr. The fast flux and neutron temperature can also be determined by adding Ni and Lu. The k0-DALAT code does not apply thermal or epithermal self-shielding corrections.

3.5.3. k0-IAEA

For determination of Φ_{th} , f and α , the code offers the use of bare monitor methods. Al-Au plus Zr, for example, or Cr, Mo plus Au, or any suitable reference material. If any element (e.g. Al, Fe or Ni) is added to yield a gamma ray peak through threshold activation, the fast flux is also determined. And if any element is added with non-unity $g(T)$ -values, such as Lu, T is determined as well.

Internally, the code uses an alternative for the Høgdahl convention, where the thermal fluence rate is defined as the integral over the entire Maxwell-Boltzmann distribution, instead of the integral up to the Cd-cutoff energy. This results in slightly higher values for the thermal fluence rate Φ_{th} than for the subcadmium fluence rate Φ_s , and slightly lower values for the epithermal Φ'_{epi} as compared to the epicadmium Φ_{epi} rate.

The following definitions and equations allow for conversion back and forth. The ‘-marks denote the k0-IAEA alternatives for the standard k_0 parameters.

$$Q'_0(0) = Q_0(0) - 0.429 \quad (27)$$

$$Q'_0(\alpha) = \frac{Q'_0(0)}{E_r^\alpha} \quad (28)$$

$$f' = \frac{\Phi_{th}}{\Phi'_{epi}} \quad (29)$$

$$f' = f + \frac{0.429}{(2\alpha+1)E_{Cd}^\alpha} \quad (30)$$

$$\Phi_s \left(g_{th}g(T) + g_{epi} \frac{Q_0(\alpha)}{f} \right) = \Phi_t \left(g_{th}g(T) + g_{epi} \frac{Q'_0(\alpha)}{f'} \right) \quad (31)$$

All of this has no impact on the mass fractions calculated in the end (as the last equation demonstrates), it is only mentioned here in case neutron spectrum parameters determined with one convention are to be compared to others, as was the case in this intercomparison.

The k0-IAEA code can fit parabolic curves to neutron spectrum parameters as a function of position in the irradiation facility, and apply them to samples automatically, but only if the samples and flux monitors were irradiated in the same irradiation container at the same time. If this is not the case, any parameter not available from the current sample irradiation is taken

from a time-sorted database of neutron spectrum parameters, without gradient correction. The user can edit the neutron spectrum parameters, if need be, in unforeseen situations.

3.5.4. k0-INRIM

The neutron spectrum parameters are determined with the ‘triple bare’ method. The experimental setup for the evaluation is locked to the situation where all spectra for monitors are acquired at the same counting position (reference position is obviously preferred) in order to minimize positioning effects since they are not considered in f and α calculations as well as monitor geometry effects (as reference sources are supposed to be point-like or thin foils). Conventional thermal, epithermal and fast fluxes can also be returned, for user information, even if they are not used in the model to calculate mass fractions. A correction for vertical flux gradient is provided based on a linear approximation and calculated using the count rate of two monitors co-irradiated with the sample. Databases collecting values for all these flux parameters are continuously updated and historical values can be recalled, if needed, or exported in Microsoft Excel files.

3.5.5. k0-IPEN

The f and α parameters can be determined by the “triple bare” method or the “Cd-cover” method using Au-Al, Zr, Zn and Fe foils.

3.6. ACTIVATION EQUATION CORRECTIONS

Over time, more and more corrections were added to the activation equation of the k_0 -NAA method. Not all participant codes have implemented them all. For true coincidence summing corrections, some participant codes rely on external software, others perform them internally.

3.6.1. KayWin

The software package includes g_{th} , g_{epi} , $g(T)$ and true coincidence summing corrections, as well as primary burnup. Any level of complexity of activation and decay is also handled.

3.6.2. k0-DALAT

The code includes $g(T)$ and primary burnup (for Au only) corrections. For true coincidence summing corrections, the code relies on external software.

3.6.3. k0-IAEA

The code includes g_{th} , g_{epi} , $g(T)$ and true coincidence summing corrections, as well as primary burnup (e.g. for ^{197}Au) and secondary activation (e.g. $^{197}\text{Au} \rightarrow ^{198}\text{Au} \rightarrow ^{199}\text{Au}$). Any level of complexity of activation and decay is also handled.

3.6.4. k0-INRIM

The code includes self-shielding corrections (g_{th} and g_{epi}) in the measurement model but their values have to be calculated by the user; conversely, the software calculates true coincidence corrections internally based on results of the detector characterization (full energy curve and peak-to-total) and literature values.

3.6.5. k_0 -IPEN

The code includes coincidence summing correction, applying the Semcow matrix algorithm, and gamma self-attenuation correction. g_{th} , g_{epi} are input parameters, calculated externally by the MATSSF code [25, 26].

3.7. INTERPRETATION

Sometimes, a single peak area translates to a single element's mass fraction without further ado. But often, other elements contribute to the same peak. Such interferences can arise from two nuclides emitting indistinguishable energies ('spectral interferences'), or from two elements yielding the same radionuclide ('primary reaction interferences'). In order to ensure that all possible interferences are dealt with, measures must be taken by the software. The k_0 -NAA method does not specify how to do this, nor does it include all reactions or peaks that might be involved.

Since threshold reactions are not included in the k_0 -NAA method, but they do take place in any sample and can interfere with (n, γ)-reactions, in that they may produce the same radionuclide for a different element, or a gamma ray energy that is close to or identical to a peak stemming from a (n, γ)-reaction, any code implementing the k_0 -NAA method can be expected to also deal with these reactions. The same applies to peaks in the spectrum that have no associated k_0 factor.

A single chemical element may yield multiple gamma ray peaks in a single spectrum, and/or multiple gamma ray peaks in spectra obtained from the same sample in different spectra, possibly after different irradiations. The k_0 -NAA method does not specify how to obtain the best estimate of an element's mass fraction from complex sets of spectra and peak areas, so each participant code may perform this task in different ways. Some may offer the user to point out the peaks to be included in or excluded from the process.

When an element is not detected, a detection limit (or upper limit) for the mass fraction can be a useful result. All participant codes offer these, based on their own methods.

Samples are often irradiated and measured with some packaging, necessitating blank corrections. All participant codes offer the possibility to perform the blank corrections.

A resulting mass fraction is useless without a specified uncertainty that covers all sources thereof, and there are many such sources. Since k_0 factors are correlated for the peaks of a given element, and results from peaks from different spectra obtained from the same sample are also correlated, uncertainty propagation is a task that is more complicated than the mass fraction calculation itself, no matter if the goal is to establish a traditional 'precision' and/or 'accuracy', a 'GUM' or an 'extended uncertainty'. All participating codes report uncertainties, each determining them in their own way.

3.7.1. KayWin

The interpretation and evaluation of the results begins with the determination of the detection limit in units of concentration (according to Curry) for all gamma lines in the library. The number of channels taken for the calculation of the background and detection limit depends on the full width at half maximum (FWHM) at that energy. Based on this, a first selection can be made of the nuclides that can be determined from the spectrum (criterion $DL < X\%$, see Fig. 1). A second selection is made using an algorithm based on multiple gamma rays emitted by the nuclide. These results are then used to correct for spectral interference [41]. An additional

check shows whether an element is present in the sample based on all of the element's nuclides and all of its measurements. Correction for epi-thermal shielding, blank, threshold activation interference (including from target elements that were not measured) and fission products can be selected manually (See Fig. 2 for all results for Mg and Fig. 3 for Sb). The uncertainty of a single gamma line is based on the counting statistic. The standard deviation of the peak area of a gamma line can be calculated by the software based on the background in that area. Average concentrations of multiple gamma lines, multiple nuclides, multiple irradiations and/or multiple measurements can also be weighted based on $1/sd^2$. The expanded uncertainty is calculated from the uncertainties in the nuclear data and measurement parameters according to Kragten's method [42].

3.7.2. k0-DALAT

The detection limit D , in counts, is computed as follows:

$$D = 2.706 + 4.653 \sqrt{B} \quad (32)$$

where B is the background be obtained by summation of the counts in n channels of the expected peak width based on $n/2$ channels at the left and $n/2$ channels at the right of the peak of interest. The combined standard uncertainty is estimated according to the law of the propagation of uncertainties of components such as sample mass, geometry, neutron flux, counting statistics (1 sigma), etc. The expanded uncertainty ($u(e)$) is used as

$$u(e) = \sqrt{s^2/n + u(com)^2} \quad (33)$$

where s is the standard deviation of n replicates and $u(com)$ is the combined standard uncertainty of k_0 -NAA.

3.7.3. k0-IAEA

The code interprets the sample spectra using linear least squares methods to solve a system of linear equations. It assumes that each measured peak area is the linear sum of contributions from, potentially, all chemical elements. To establish the magnitude of the contributions, for each element it calculates the peak areas that would have been measured if the mass fraction of the element had been 100% for all spectra obtained from the sample, even if it was irradiated and measured repeatedly. In this step, it takes all types of activation reactions and all kinds of peaks in the spectrum into account. Uncertainties in k_0 factors as well as all other sources of peak-specific uncertainty are propagated to these predicted peak areas, as if they were uncorrelated. For peaks without associated k_0 factors, a 20% uncertainty is assumed.

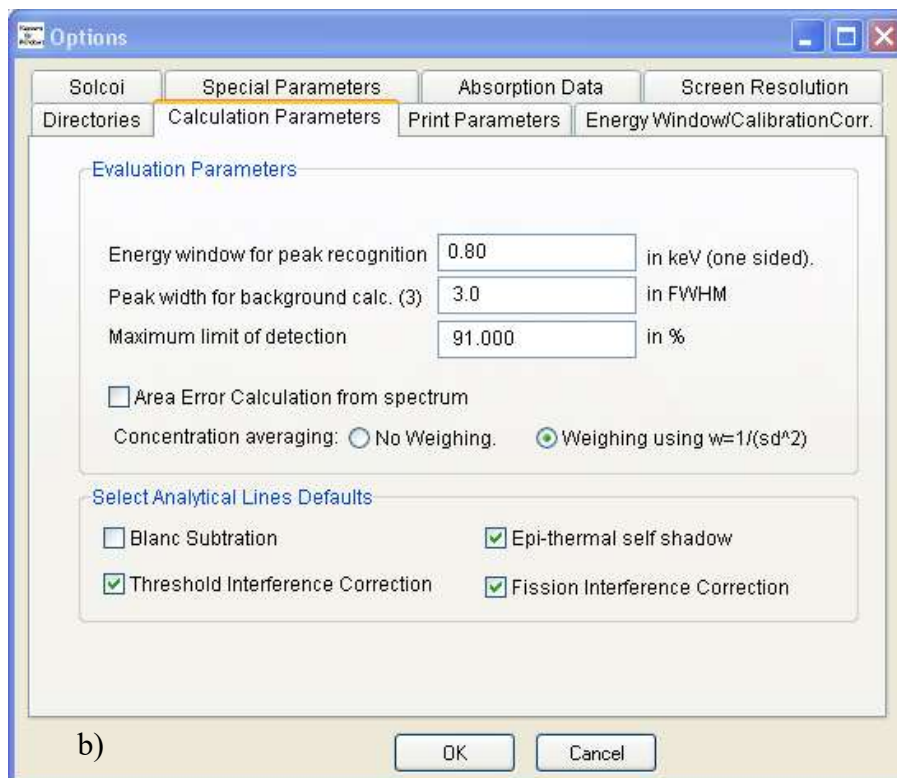
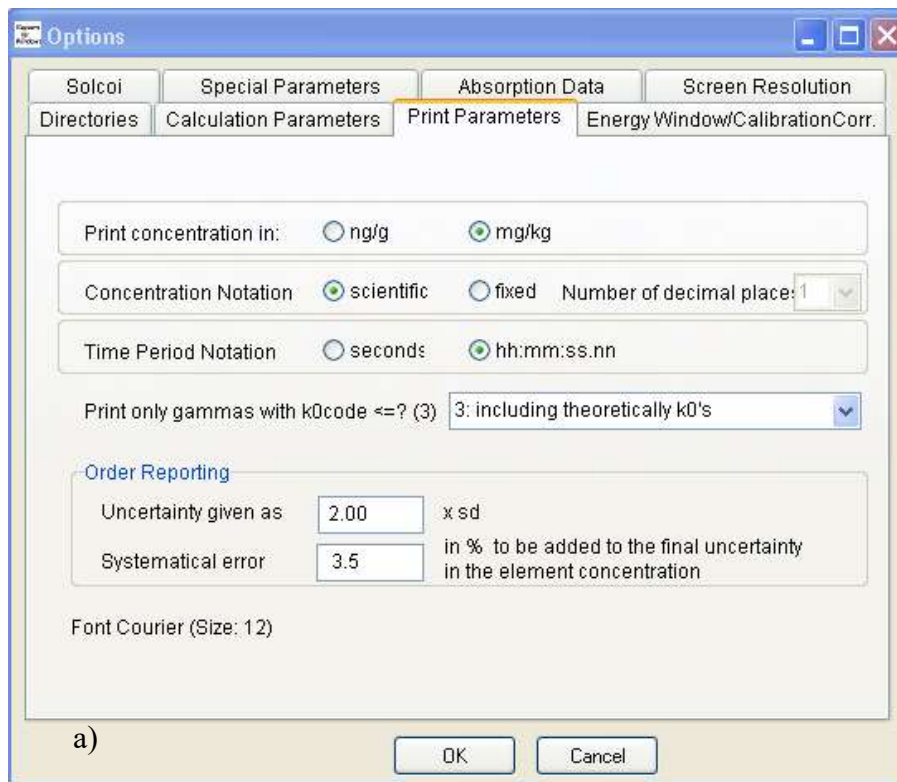


FIG. 1. a) Print parameters (top) and b) evaluation in KayWin (bottom).

Usually, there are more detected peaks than related unknown mass fractions, so that the system of linear equations has more equations than unknowns. It can then be solved by standard linear least squares methods, where at first only the Poisson-derived uncertainties in the peak areas are taken into account to find the least-squares solution. After the first solution has been computed, it is employed to propagate the uncertainties in the predicted peak areas to the

measured peak area uncertainties, and the linear least squares procedure is repeated. The uncertainties in the mass fractions resulting from the first step are named ‘precision’, because they only reflect counting statistics and can only serve to forecast repeatability of the measurement result. The uncertainties in the mass fractions from the second step are named ‘accuracies’, because they should indicate how close the reported mass fraction is to the truth.

In this way, the code calculates optimum results (in the linear least squares method sense of the word), while taking all possible interferences and all available information into account simultaneously. When an element yields interference-free peaks exclusively, the process boils down to a kind of weighted averaging.

Uncertainties in f and α are propagated by repeating the entire process with modified values, where f is increased with its own uncertainty and α decreased with its own uncertainty, to account for the strong negative correlation between these two, stemming from the use of the bare monitor method.

Once the mass fractions have been determined, sample-specific uncertainties (e.g. sample mass, thermal neutron fluence rate or irradiation time) are simply propagated to all mass fractions. More detail is given in Refs [6] and [7].

The code estimates detection limits from the continuum in the spectrum by calculating the peak area that would have a 95% probability of being detected, given the peak width and the peak-search threshold settings. From that area, a mass fraction can be calculated that is reported as the detection limit (that mass fraction, if it was present and detected, would then end up being reported with an uncertainty of 25%, assuming a peak-search threshold of two standard deviations).

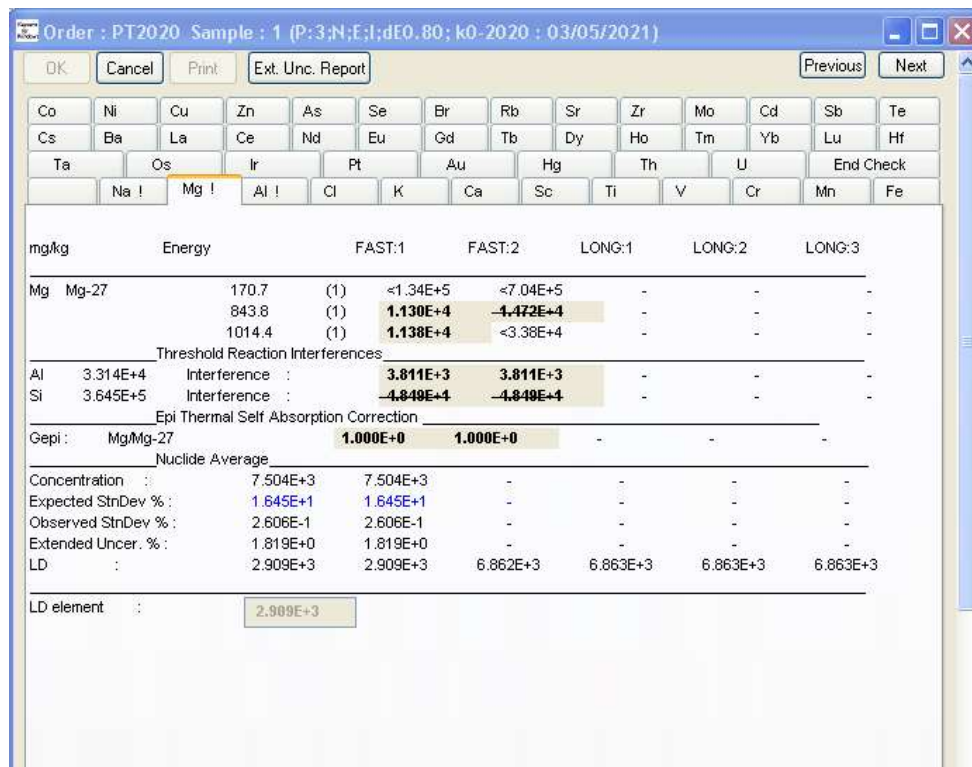


FIG. 2. KayWin: Summary and user input screen for result evaluation with the ability to (de)select lines or corrections for Mg.

Order : PT2020 Sample : 1 (P:3;N:E;l;dE0.80; k0-2020 : 03/05/2021)

OK Cancel Print Ext. Unc. Report Previous Next

mg/kg	Energy	FAST:1	FAST:2	LONG:1	LONG:2	LONG:3
Sb Sb-122	564.2 (1)	<1.37E+3	<3.97E+2	1.059E+0	1.074E+0	<2.42E+0
-> without interfer. corr.						
Epi Thermal Self Absorption Correction						
Gepi : Sb/Sb-122	-	-	1.000E+0	1.000E+0	-	-
Nuclide Average						
Concentration :	1.072E+0	-	-	1.059E+0	1.074E+0	-
Expected StnDev % :	1.672E+0	-	-	4.526E+0	1.799E+0	-
Observed StnDev % :	4.870E-1	-	-	-	-	-
Extended Uncer. % :	2.994E+0	-	-	2.994E+0	2.994E+0	-
LD :	4.267E-2	1.376E+3	3.979E+2	4.285E-1	4.267E-2	2.423E+0
Sb Sb-124	602.7 (1)	<5.26E+4	<1.52E+4	<4.69E+0	1.157E+0	1.151E+0
	645.9 (1)	<7.02E+5	<1.97E+5	<6.50E+1	<2.06E+0	<1.68E+0
	722.8 (1)	<4.73E+5	<1.21E+5	<4.71E+1	4.447E+0	4.667E+0
-> without interfer. corr.						
	1691.0 (1)	<1.34E+5	<2.78E+4	<1.09E+1	1.182E+0	1.187E+0
	2090.9 (1)	<5.82E+5	<2.09E+5	<1.31E+2	1.003E+0	1.342E+0
Epi Thermal Self Absorption Correction						
Gepi : Sb/Sb-124	-	-	1.000E+0	1.000E+0	1.000E+0	-
Nuclide Average						
Concentration :	1.163E+0	-	-	-	1.161E+0	1.164E+0
Expected StnDev % :	7.200E-1	-	-	-	1.138E+0	9.296E-1
Observed StnDev % :	6.971E-1	-	-	-	1.248E+0	1.727E+0
Extended Uncer. % :	2.885E+0	-	-	-	2.881E+0	2.887E+0
LD :	8.385E-2	5.268E+4	1.525E+4	4.698E+0	1.257E-1	8.385E-2
Element Average						
Concentration :	1.147E+0	-	-	1.059E+0	1.133E+0	1.164E+0
Expected StnDev % :	6.616E-1	-	-	4.526E+0	9.626E-1	9.296E-1
Observed StnDev % :	9.428E-1	-	-	-	2.159E+0	1.221E+0
Extended Uncer. % :	2.904E+0	-	-	2.994E+0	2.917E+0	2.887E+0
LD element :	4.267E-2	1.376E+3	3.979E+2	4.285E-1	4.267E-2	8.385E-2
Other Nuclide LDs						
Sb Sb-124m	LD :	6.784E+3	1.152E+4	-	-	-

FIG. 3. KayWin: Summary and user input screen for evaluation of the result with option to (de)select lines or correction for Sb.

The code corrects for blank, if a blank has been indicated and the known composition entered.

A special property of the code is that it will allow for negative mass fractions as the outcome of the interpretation process. This may seem counterintuitive, but forcing positive outcome will bias results in a manner that becomes noticeable if repeated measurements are performed of a mass fraction that is well below the detection limit.

3.7.4. k0-INRIM

The software provides, for a certain target element, n uncertainty budgets for as many peak areas obtained from the sample. Thus, in case more than one peak is associated to the same target, the corresponding uncertainty budgets are reported in the Excel output independently; therefore, it is the user task to inspect the Microsoft Excel output and select, discard or average the results obtained for the same target in the most suitable way.

The combined uncertainty reported in the budget is based on a first order Taylor series approximation of the measurement model $y = f(x_1, x_2, \dots, x_i, \dots, x_n)$, where x_i is the i -th of the n input parameters. It is obtained by propagating covariances of input parameters using sensitivity

coefficients calculated by evaluating variations of y due to $\pm u(x_i)$ changes. The uncertainty budget includes information of all input parameters such as symbol, unit, value, standard (absolute and relative) uncertainty, sensitivity coefficient, correlation matrix, covariance matrix and the measurement model. In addition, the index of the contribution to the combined uncertainty of each input parameter is given to help user identifying the most overriding ones.

The Microsoft Excel output budget includes input cells to correct for γ -interferences (spectral and reaction) that are not automatically evaluated. Currie's detection limits are calculated based on eq. 5.61 of Ref. [43]; background values are approximated through the integral of background peaks within a range of 3FWHM (FWHMs are internally calculated during the detector characterization).

3.7.5. k0-IPEN

The detection limit D is taken from Ref. [44], applying the Paired Measurement methodology and using the following equation:

$$ky = \frac{(k + \sqrt{8n_b})}{1 - (ku_{rel}(y))^2} \quad (34)$$

where

k is the coverage factor

n_b is the background counts.

u_{rel} is the relative uncertainty of y , and

y is the value of the conversion function, including the measurement time.

The calculation considers the original spectrum in a region near the peak of interest.

3.8. FEEDBACK TO USER AND REPORTING

Even when automated to a great extent, all kinds of things can still go wrong in INAA. It is therefore important to provide the user with feedback that shows intermediate results and internal discrepancies, both during the interpretation and afterwards. One source of mistakes can be the copying of analysis results to report documents, so some participant codes offer customizable report formats. For QA/QC purposes, it can be desirable to present results for reference materials and blanks along with certified or known values in a report. A code can even keep track of previous results and inspect for outliers or trends.

3.8.1. KayWin

All intermediate results can be displayed and printed (see Figs. 2 and 3). Efficiency measurements and multimonitor calibrations can be plotted in graphs. A control chart of comparator factors, efficiency, energy calibration can be plotted. The analysis result based on all measurements is displayed by element, as in Fig. 2 for Mg and Fig. 3 for Sb. Using the space bar, a line or correction can be selected or deselected. As an additional check, the detection limit of unidentified nuclides is also shown (^{124m}Sb).

After validating the results, a report can be created with one concentration per element, including uncertainty based on counting statistics, including a standard expanded uncertainty or calculated expanded uncertainty if needed, with desired uncertainty level.

3.8.2. k0-DALAT

The code results in two formats of the final report, i.e. a text format for easy reading, and another format compatible with Excel spreadsheet.

3.8.3. k0-IAEA

The code strongly relies on graphics to inform the user. Typically, measured data are plotted along with fitted curves or interpretation results, with a separate graph showing standardized residuals (i.e. the difference between measured and fitted value, divided by the uncertainty in the measured value). In the residual plots, the green colour indicates values between -2 and +2, orange between -3 and -2 or +2 and +3, and red indicates values below -3 or above +3. One in 20 residuals is expected to be 'orange', 1 in 1000 is expected to be 'red', if everything is perfectly under statistical control. Examples from the current intercomparison are shown below in Figures 4 to 7 (except for the peak in Fig. 4, since all participant codes were given the same peak areas to work with in the intercomparison), which are screen shots from the software and shown here for illustrative purposes of the different fits done by k0-IAEA.

The windows shown in Figs 4 and 7 are interactive in the software. The user can introduce additional peaks or access the fitting parameters when determining peak areas. After interpretation, the user can obtain information on the assignment of a specific peak by right-clicking on that peak, or jump to the peak fit if suspicions should arise. Peaks can also be in- or excluded from the interpretation process through this graphical interface. At the same time, the code writes intermediate results to log .txt files, and refers the user to those files in case the code itself detects trouble. If a reference material or a blank has been analysed and reported repeatedly, the code can show results from different analysis runs in trend plots and overviews.

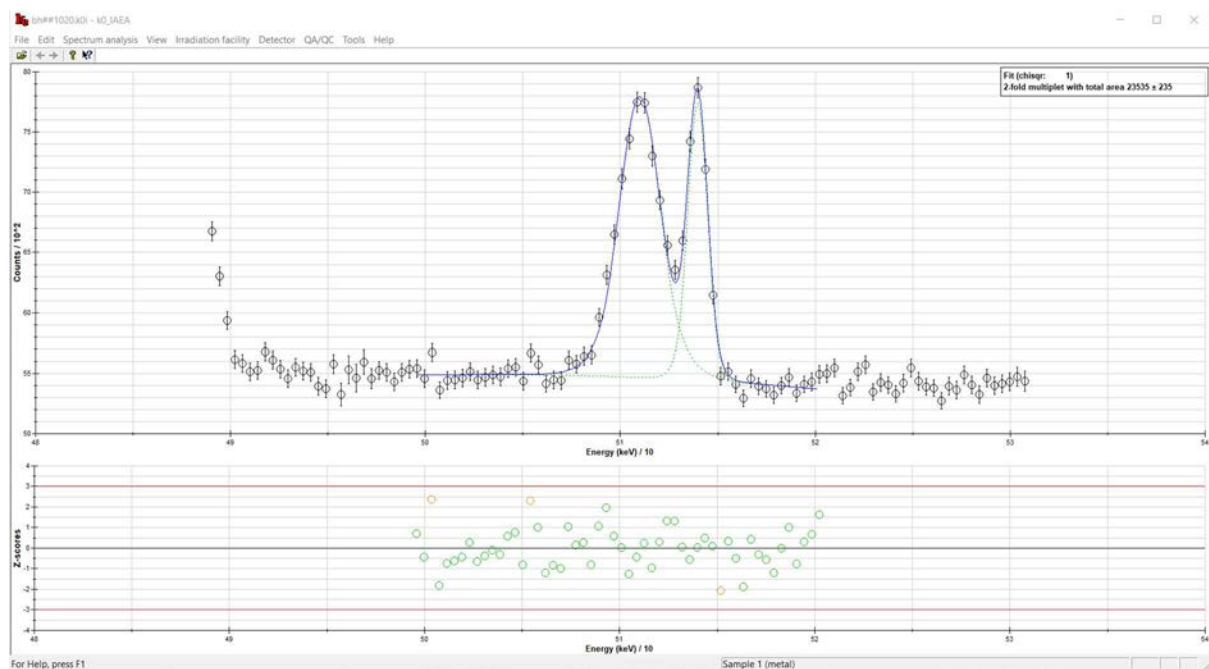


FIG. 4. k0-IAEA: Result of a peak fit at 511 – 514 keV fit. The top graph shows measured channel contents as well as the fitted curves, the bottom graph shows standardized residuals as function of energy. Notice the different peak widths used, due to Doppler broadening of the 511 keV.

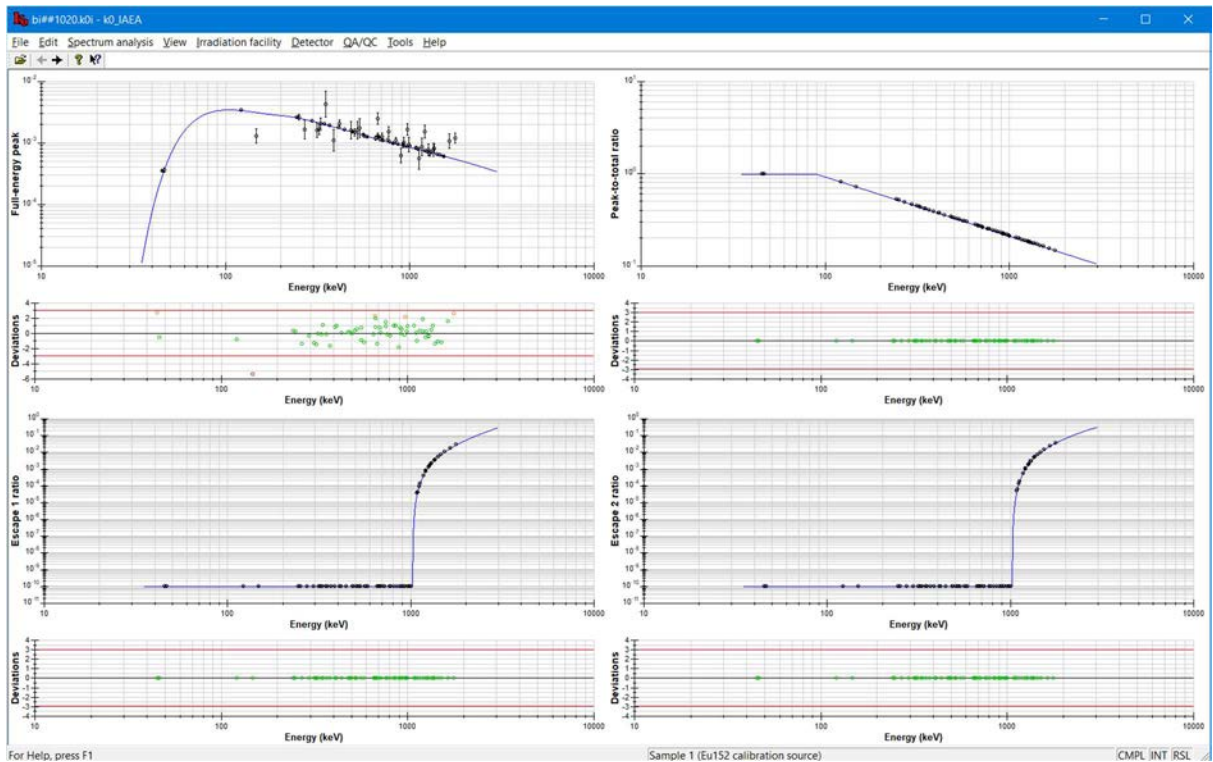


FIG. 5. Efficiency curve fit (efficiency as function of energy). The upper left graph was just fitted and shows full energy peak efficiency and meaningful, non-zero residuals. The upper-right graph is the peak-to-total curve. The lower two are the single- and double escape ratio curves.

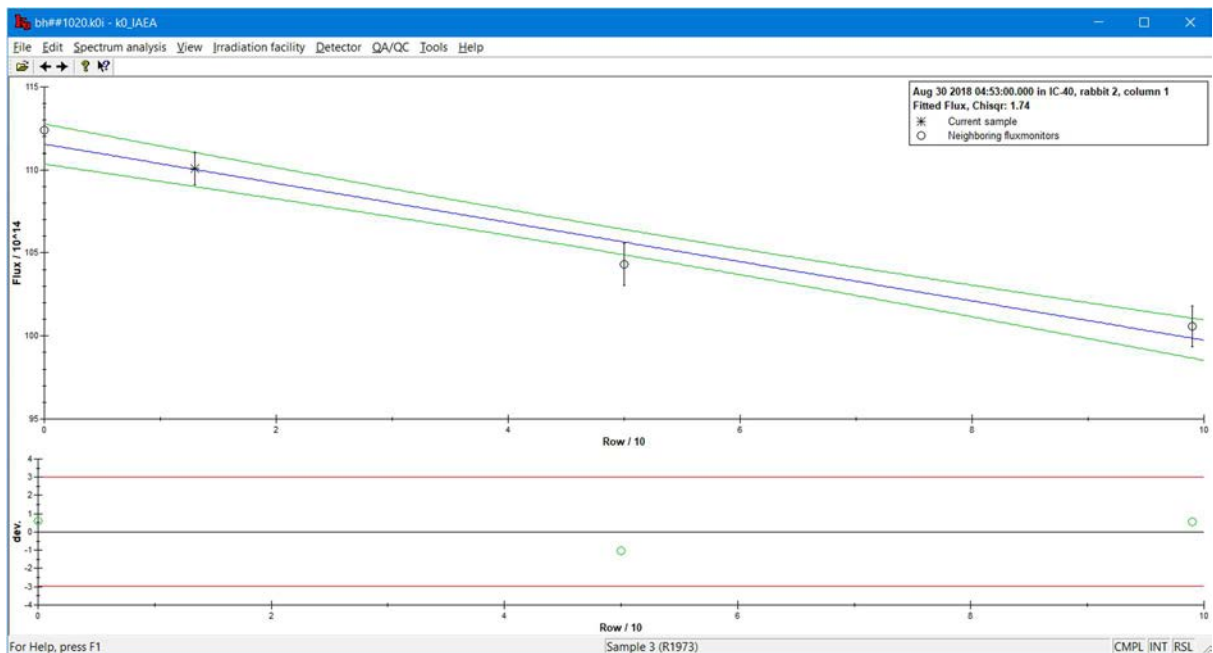


FIG. 6. Neutron fluence rate gradient fit, as a function of vertical position in mm — a straight line was fitted to the three data points because the code established that a parabola was superfluous. The green lines indicate the uncertainty in the fluence rates obtained from the fitted curve.

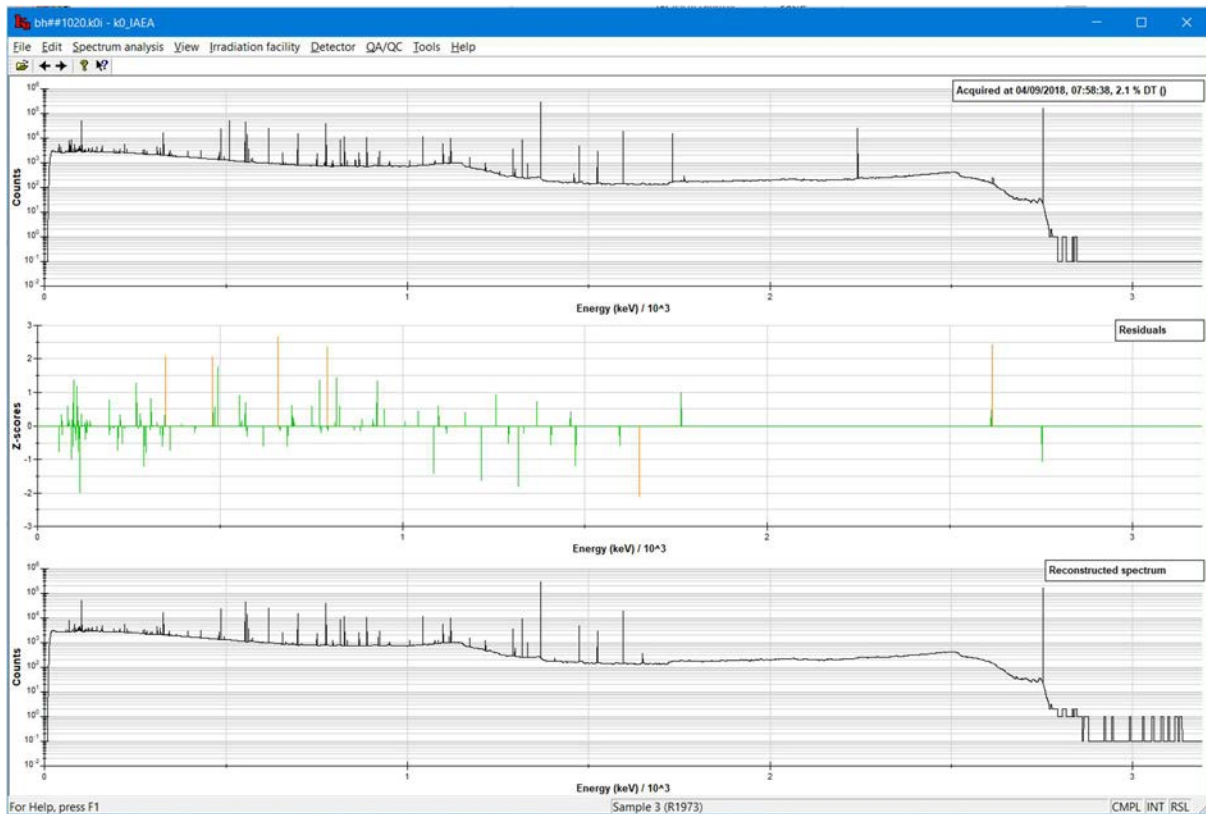


FIG. 7. Sample spectrum interpretation fit. The upper graph is the measured spectrum (yield as function of energy), the lower graph was reconstructed from the spectrum continuum and the peak areas calculated from the mass fraction results. The middle graph shows the residuals, indicating a statistically perfect agreement between measurement and interpretation result.

The code offers customizable report formats, including one that allows for easy export to Excel. When a reference material or blank is reported, it will compare the measured mass fractions with certified or known values.

3.8.4. k0-INRIM

The user-interface of the software was designed to give intermediates outputs during the data processing. Graphs, tables, text logs and entries help users to carry out the analysis step by step from the input of collected gamma spectra to the output of uncertainty budgets.

Information about fundamental steps are displayed with detailed summaries of the selected input and obtained results. This is the case for the detector characterization, flux parameters and gradient determination. The overview of the selected spectra with information of the assigned peaks can also be recalled. Moreover, before saving the results on disc, various reports are provided to the user in order to help investigating contributors to the uncertainty and the consistency of the obtained results with respect to other emissions from the same target or a reference material, if available.

Display windows of detector characterization, peak-to-total evaluation, neutron flux evaluation and peak identification are shown in Figures 8–11, respectively. In addition, output report windows including whole analysis, by spectrum analysis, by element analysis (I and II) and certified elements comparison (I and II) are displayed in Figures 12–17, respectively. Automatic blank correction is also implemented and reported in the output uncertainty budget.

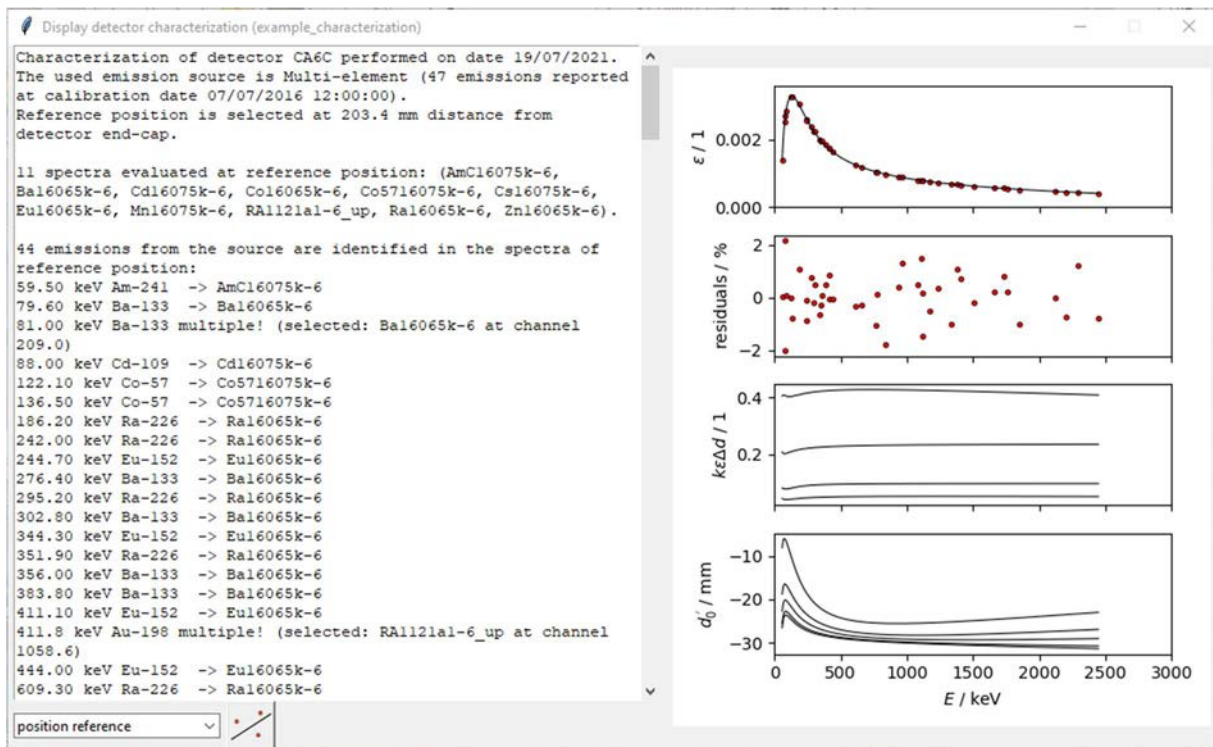


FIG. 8. Detector characterization display window; all key information and graphics for saved characterization can be recalled from the main window; information concerning all characterized counting positions can be displayed here.

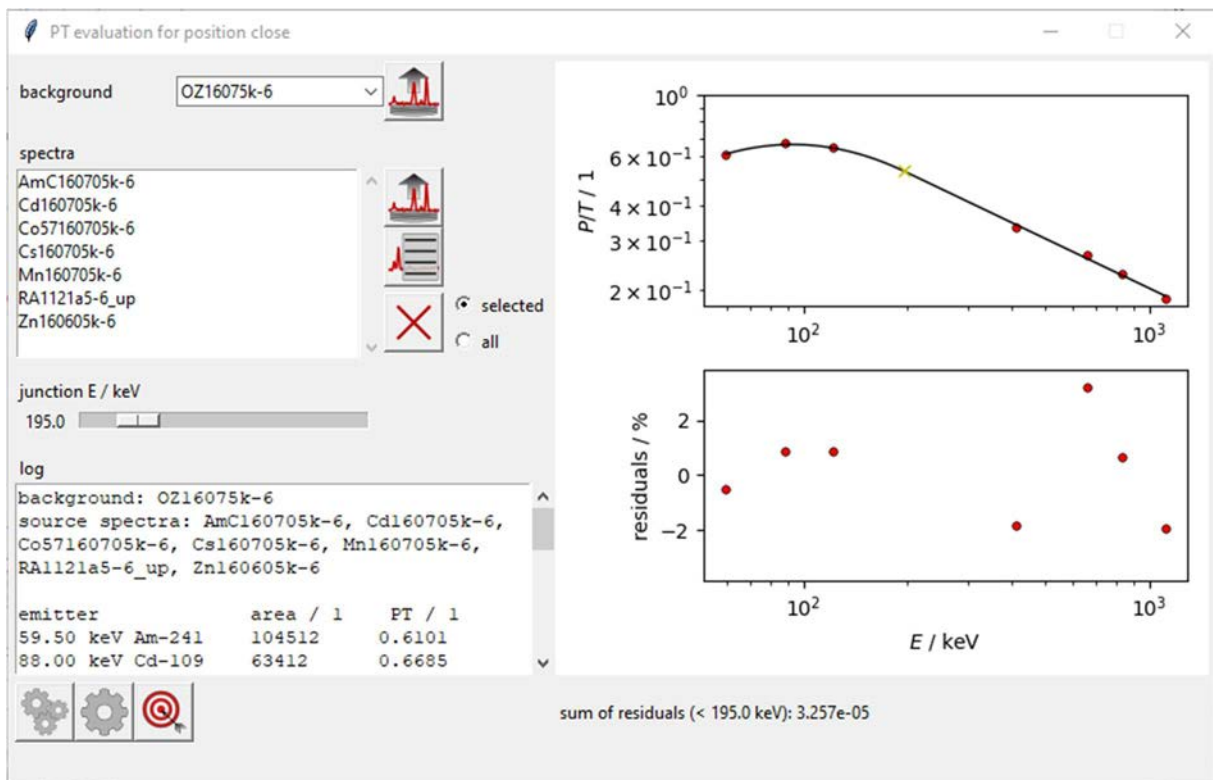


FIG. 9. Peak to Total evaluation window; information log and graphics are displayed during evaluation of peak-to-total curves. However, unlike detector characterization, the content of log box and graphics are not persistent as they are not saved on disc upon the end of elaboration process.

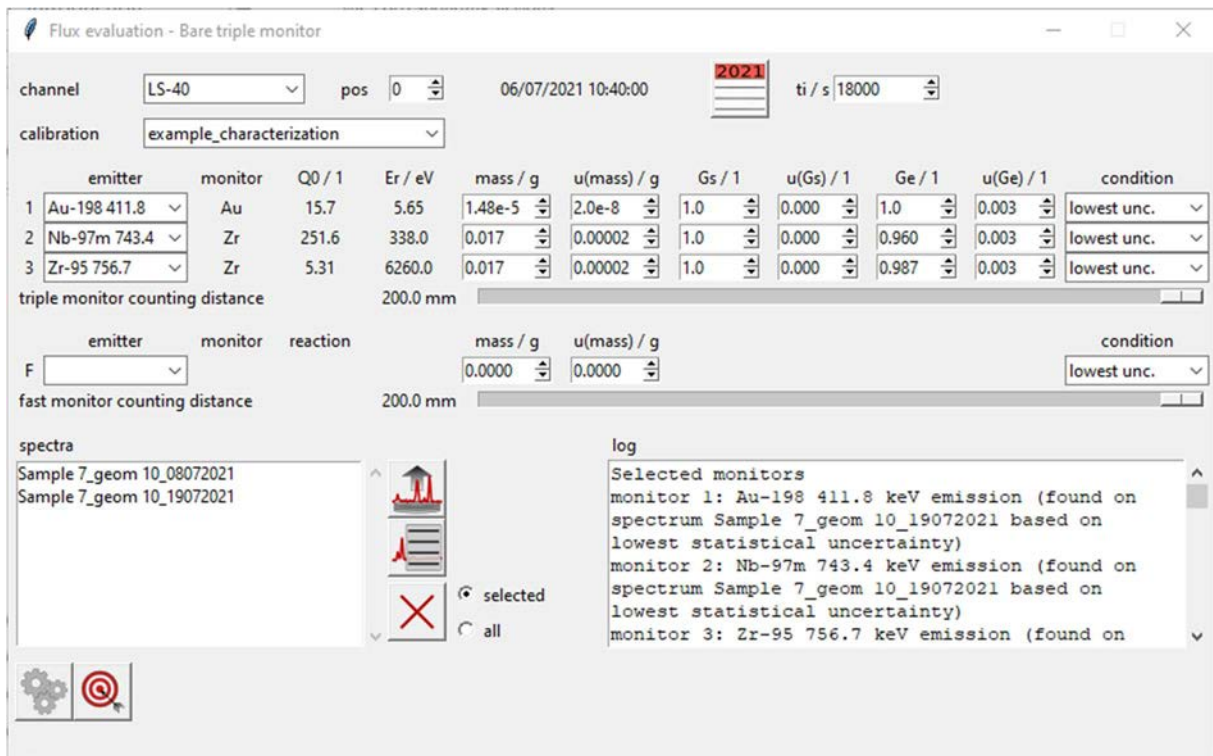


FIG. 10. Flux evaluation (bare triple monitor) window; an information log is displayed while performing neutron flux parameters and gradient evaluations. The content of log box is not saved on disc upon completion of the evaluation process.

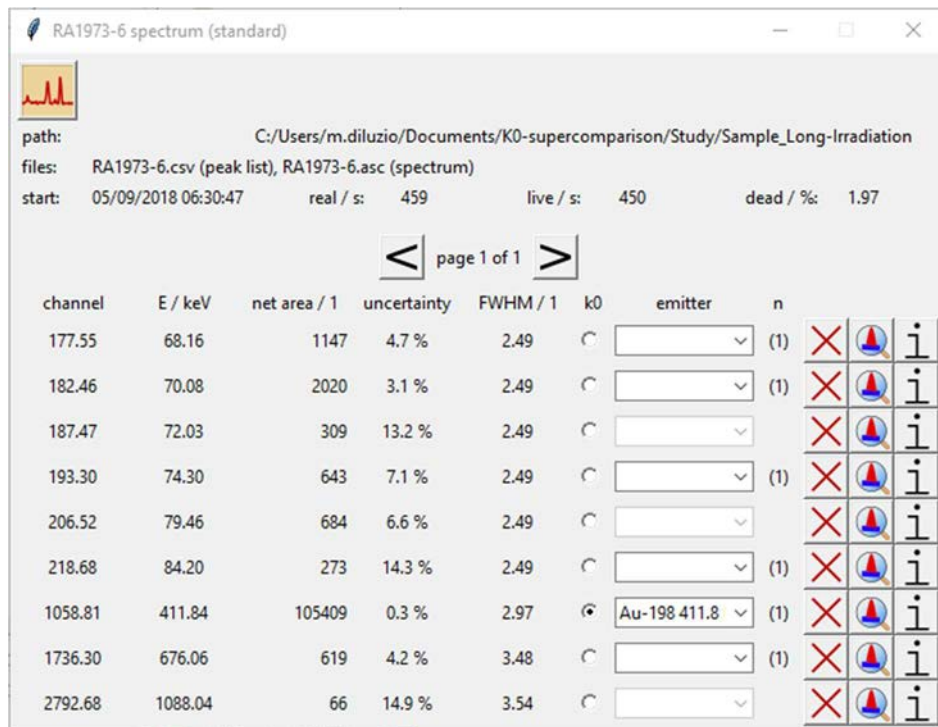


FIG. 11. Peak identification window; automatic or manual identification is performed by selection of the suspected emitter from the column 'emitter'. The label containing the name of the identified emission is reported while the value in parenthesis under the column 'n' indicates the number of entries from the k_0 database matching the energy of the peak centroid (under the column 'E / keV').

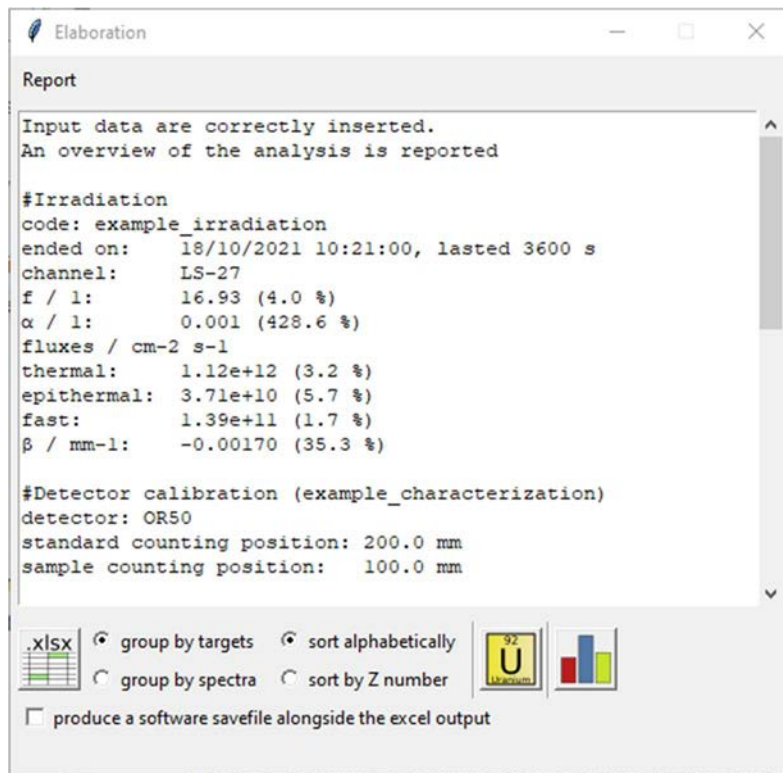


FIG. 12. Analysis report window; this window summarizes all key input parameters and informs the user about the expected results. From this window it is possible to inspect the resulting values (U button), compare values with reference material certificate (bar chart button) or saving uncertainty budgets in a Microsoft Excel output report file (xlsx button).

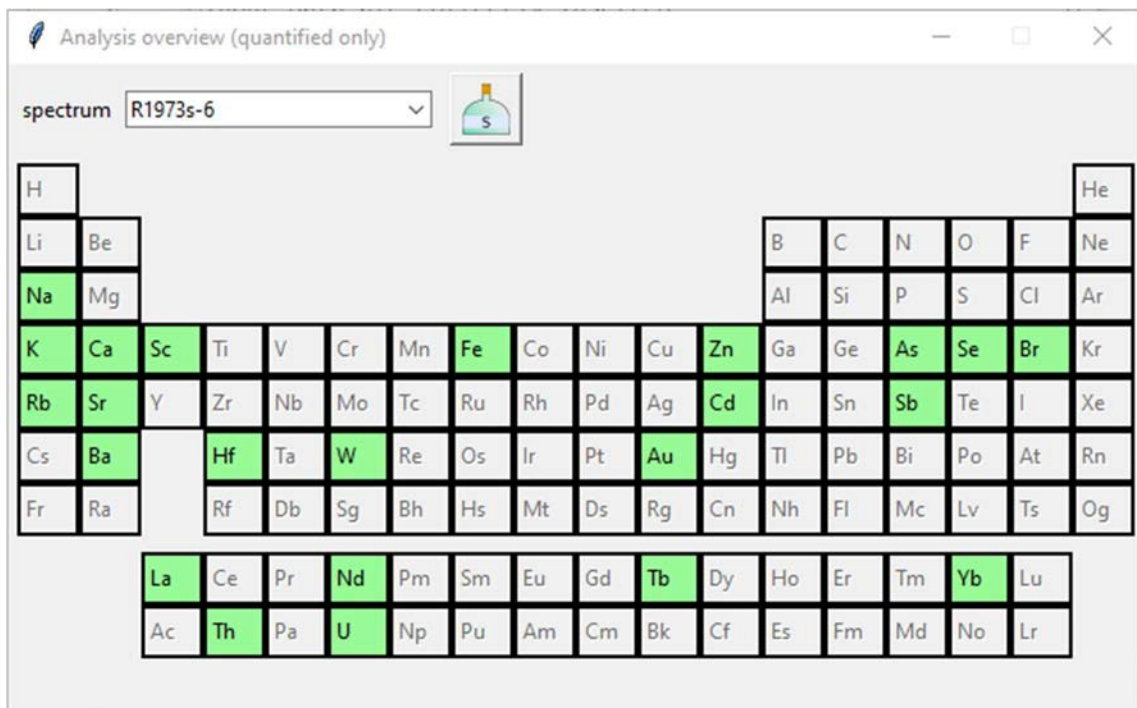


FIG. 13. Spectrum analysis overview window; this window displays a summary, by spectrum, of the elements quantified in the analysis. The green-highlighted boxes are interactive and show information about mass fraction measurements for the specific element.

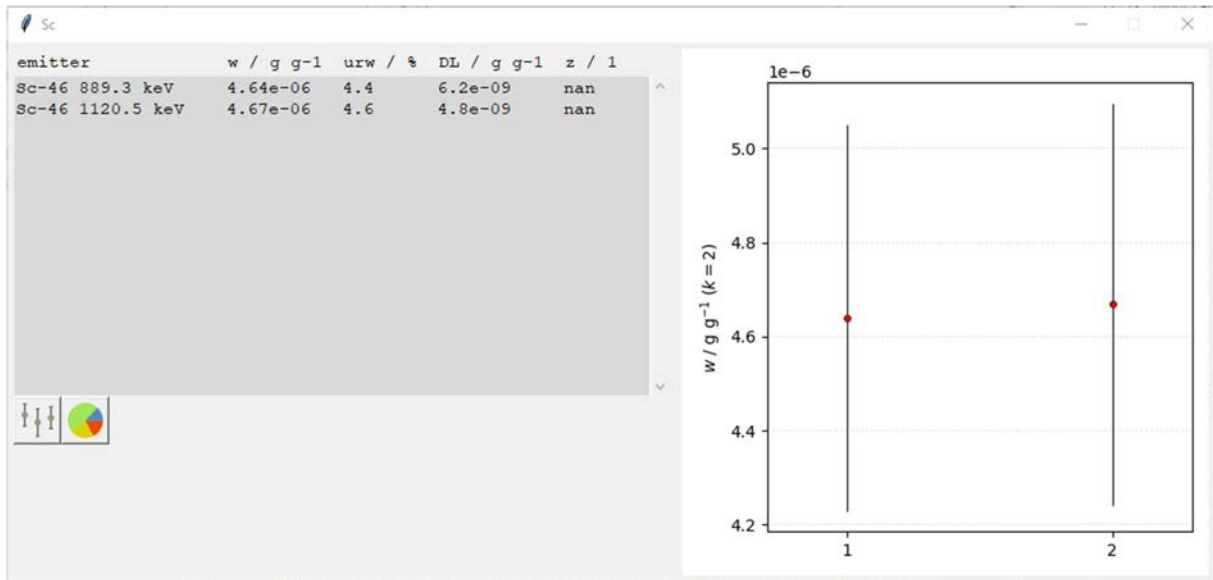


FIG. 14. Element analysis overview window (I); here are reported all mass fraction measurements, by target element, evaluated with peak areas collected from a single spectrum.

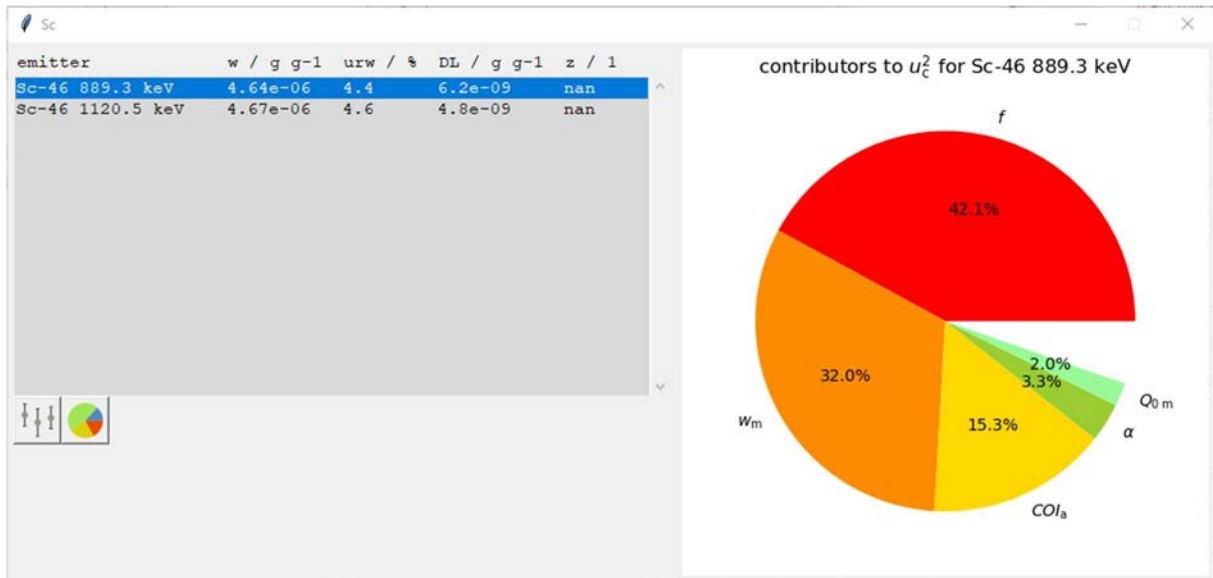


FIG. 15. Element analysis overview window (II); here are reported the 5 most important contributors to the combined uncertainty for the selected mass fraction measurement. Q_{0m} is the ratio of the resonance integral (for a $1/E$ neutron spectrum in the epi-cadmium region) to the thermal cross section of the target monitor; COI_a is the true coincidence correction factor of the target analyte (in the measurement sample); and w_m is the mass fraction of the monitor element (in the standard sample).

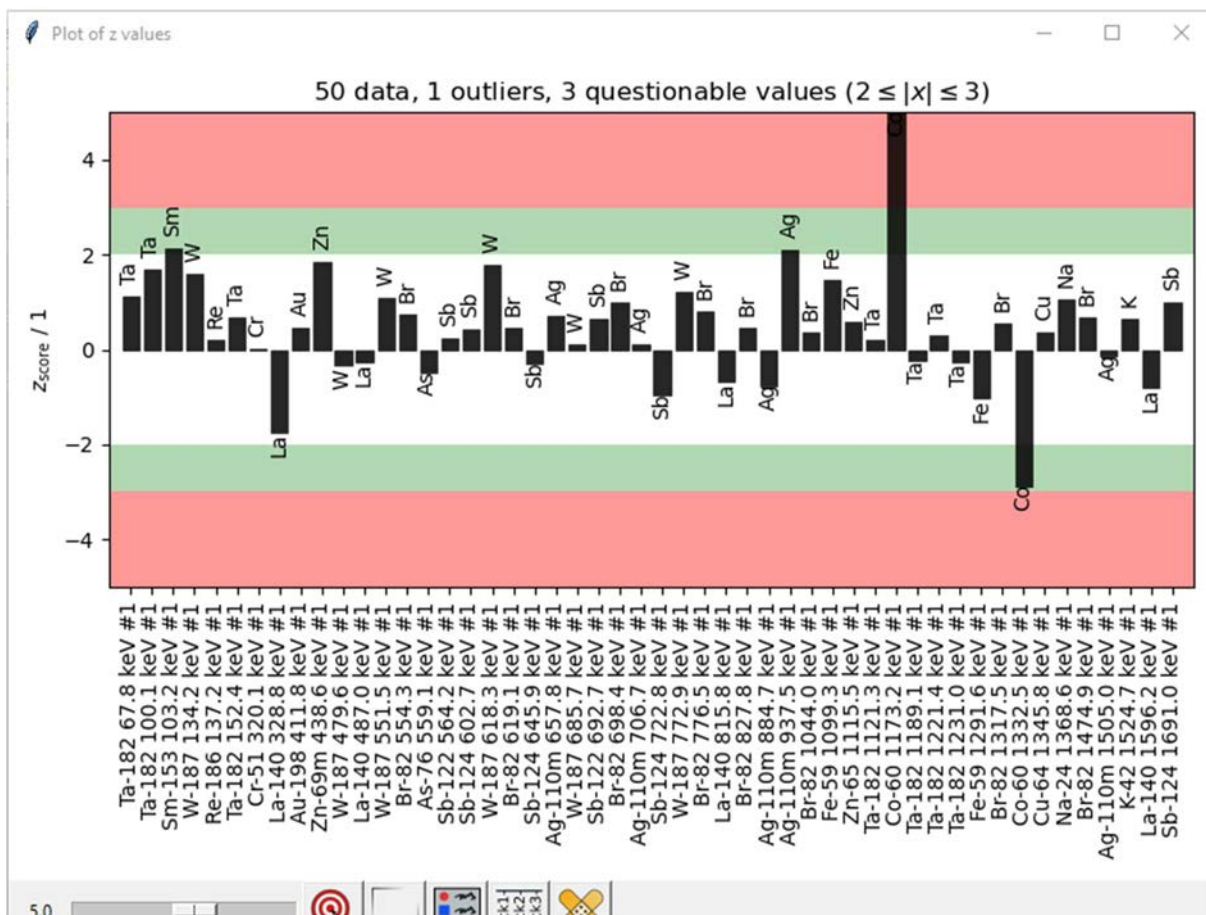


FIG. 16. Certified elements comparison window (I); in case a reference material is used as sample, automatic comparison with reference certificate values are reported as z-score barchart.

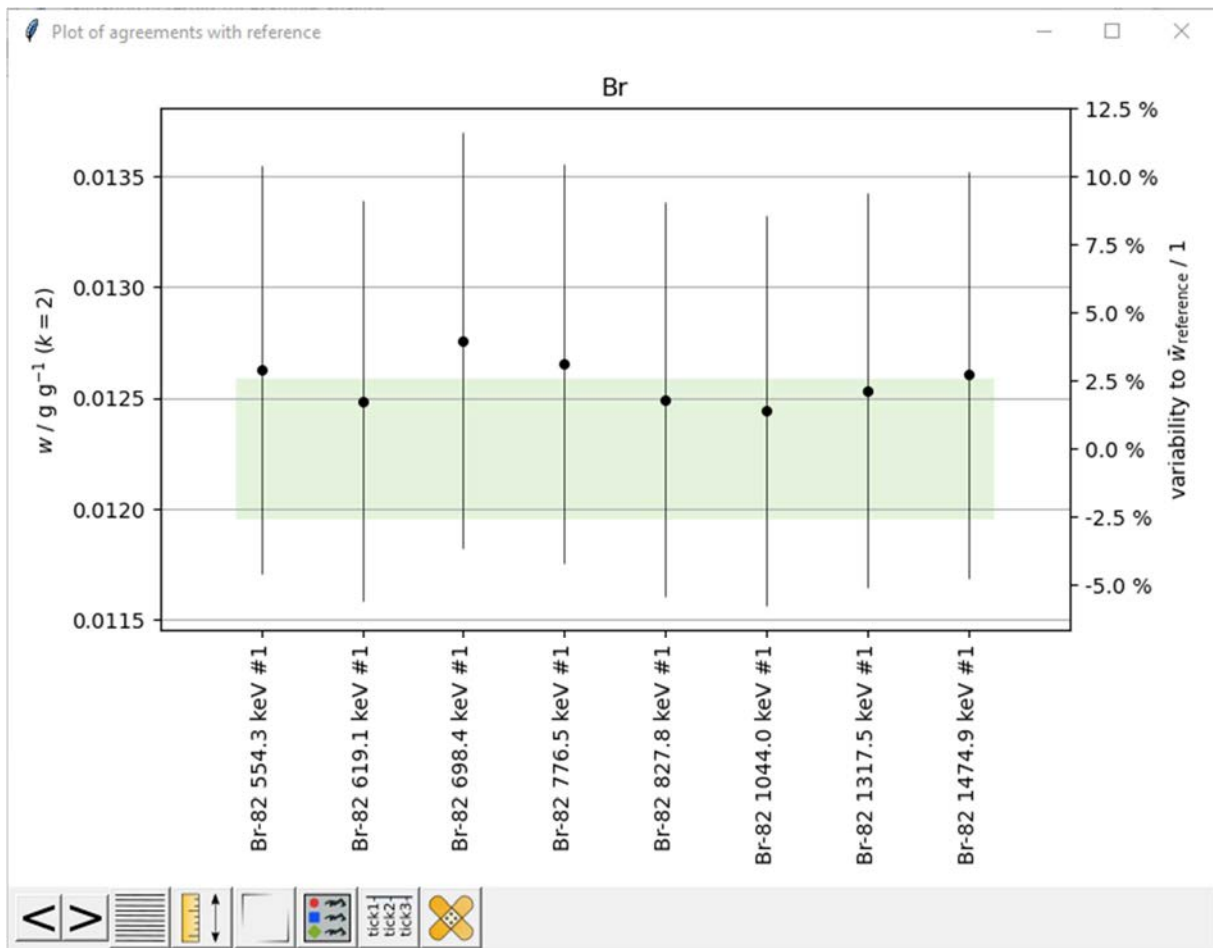


FIG. 17. Certified elements comparison window (II); in case a reference material is used as sample, automatic side-by-side comparison with reference certificate values are reported as dispersion plots for each target element.

3.8.5. k0-IPEN

The code reports in a text file the values of all parameters in order to check for possible inconsistencies. All routines keep track of partial results to be compared with the main code. All partial uncertainties are included in these reports.

3.9. ADDITIONAL FEATURES

3.9.1. KayWin

The code can give an indicative summary of the activity of samples after a given cooling period, as shown in Figure 18. In case the peak fitting code adds additional peaks to better fit a broad peak, the user can combine these extra fake peaks in the main peak using an interactive option that determines these extra peaks. The user can also correct the energy calibration of single or multiple spectra if needed. For increased accuracy the relative method can be used for a set of elements/nuclides/lines.

Activity per Nuclide				
Activity after 1 year after irradiation, higher than 100 Bq.				
Nuclide	Activity [kBq]	Date	RE	
Co-58+	0.48	31/08/19	9.608E-12	
Co-60	0.12	31/08/19	4.4618E-9	
Tb-160	0.39	31/08/19	2.5643E-6	
Zn-65	0.12	31/08/19	3.3656E-7	

FIG. 18. Screen shot of indicative summary of the activity of samples after a given cooling period.

3.9.2. k0-DALAT

No additional features are offered by k0-DALAT.

3.9.3. k0-IAEA

The code can run in fully automatic batch mode, from peak area determination to reporting. It can import sets of experimental information and spectra using spreadsheets. When installed properly, context-sensitive help will pop up when pressing function key F1.

A manual is available as a .pdf file, as well as an animated tutorial with voice-over, to instruct new users on how to get started with the software.

3.9.4. k0-INRIM

Additional features of the software are described in the manual available at the k0-INRIM software github online repository [45].

3.9.5. k0-IPEN

The code is fully automated. The input/output and executable files for each routine are organized in a structured directory system, allowing easy access to individual results. The main directory is split in subdirectories where the routines are located. Easy transfer to other machines is made by copying the whole main directory and running, with no dependence on files located at the original machine. A manual is available which is continuously updated as the code is improved.

3.10. OVERVIEW OF FEATURES

In Table 1, an overview is presented of the implemented features in the participating codes, as described in this chapter. The 'k0' column denotes features generally accepted as being integral components of the k0-NAA method.

TABLE 1. IMPLEMENTED FEATURES IN THE PARTICIPATING CODES

Feature	k_0	KayWin	k0-DALAT	k0-IAEA	k0-INRIM	k0-IPEN
General gamma ray spectrometry						
Determination of peak areas and energies from spectrum channel contents			x	x		
Dead-time correction		x	x	x	x	
Spectral background correction		x	x	x		x
Handling of random summing (i.e. at high count rates) peaks						
Detector characterization						
Determination of full energy detector efficiency curve	x	x	x	x	x	x
Determination of peak-to-total efficiency curve	x	x		x	x	x
Determination of full energy detector efficiency curve in the presence of true coincidence summing (e.g. close to the detector, or inside a well-type detector)				x		
Efficiency conversion for non-point sources and larger samples close to the detector	x	x		x	x	x
Irradiation facility characterization						
Determination of f and alpha using Cd-ratio multi-monitor method	x	x				x
Determination of f and alpha using Cd-covered multi-monitor method	x	x	x			x
Determination of f and alpha using bare multi-monitor method	x	x		x	x	x
Determination of f and alpha using bare 3-monitor method using Zr and Au	x	x	x	x	x	x
Automatic flux parameter interpolation when gradient is present				x	x	
Determination of T (for non 1/v reactions)	x	x	x	x		
Determination of fast neutron fluence rate or fast flux ratio		x		x	x	
Activation equation corrections						
Complex activation and decay correction	x	x	x	x		
Activation and decay correction for variability of neutron fluence rate/intermittent irradiation	x	x		x		
Thermal neutron self-shielding correction (g_{th})	x	x		x		x
Epithermal neutron self-shielding correction (g_{epi})	x	x		x		x
Non-1/v activation ($g(T)$)	x	x	x	x		
Primary burnup	x	x		x		
Secondary burnup				x		
True coincidence correction c	x	x		x	x	x

TABLE 1. IMPLEMENTED FEATURES IN THE PARTICIPATING CODES (CONT.)

Feature	k_0	KayWin	k0- DALAT	k0- IAEA	k0- INRIM	k0- IPEN
Interpretation						
Use all nuclides in the k_0 -library	x	x	x	x	x	x
Include single and double escape peaks		x		x		
Include pure sum peaks				x		
Include threshold capture reactions						
Relative method for selected nuclides (optional)		x			x	
Correction for primary reaction interferences included	x	x	x	x		
Correction for fission reaction interferences included	x	x		x		
Correction for irradiation container blank included	x	x		x	x	x
Correction for threshold reaction interference included	x	x	x	x		
User can select analytical lines		x	x	x	x	x
Automatic combination of results from different peaks of the same element within a spectrum						
Automatic combination of results from different spectra of the same sample		x		x		
Determination if a nuclide or element is present in the sample (multiple measurements/irradiations)		x	x	x		
Extended uncertainty calculation		x		x	x	x
Limit of detection calculation, especially in an area in the spectrum without peaks		x	x	x	x	x
Reporting						
Reports of all intermediate steps available		x		x	x	
Automatic reporting of comparison of reference material results with comparison to certified values				x	x	
Automatic reporting of comparison of blank results with comparison to known values				x		
Customization of report format				x		
Applicability						
Thermal INAA	x	x	x	x	x	x
Epithermal (cadmium-covered) NAA	x	x	x	x		x
Low-energy photon detector	x					
Prompt-gamma NAA				x		

TABLE 1. IMPLEMENTED FEATURES IN THE PARTICIPATING CODES (CONT.)

Feature	k_0	KayWin	k0- DALAT	k0- IAEA	k0- INRIM	k0- IPEN
Other features						
Automated input of multiple measurement from inputfile		x	x	x		
QA/QC trend analysis of ref.mat. or blank results				x	x	
Manual available				x	x	
Context-sensitive help available when in use				x	x	
Tutorial available				x	x	
Nuclear data						
Uses standard k_0 factors and nuclear parameters	x	x	x	x	x	x
Allows use of alternative database?			x		x	
Allows user editing of constants?						
Specifies which (version of the) k_0 database was used, or can show the actual parameter values used		x	x	x	x	x

3.11. ACCEPTED FILE FORMATS

In Table 2, an overview is presented of the file formats that the participating codes accept as input. In the table, ‘x’ denotes accepted input, ‘X’ denotes preferred input.

TABLE 2. SPECTRUM FILE FORMATS ACCEPTED BY THE PARTICIPATING CODES

	extension	KayWin	k0-DALAT	k0-IAEA	k0-INRIM	k0-IPEN
Spectrum file formats						
Aptec spectrum files	*.ap0		x	x		
Aptec v4.3 spectrum files	*.a43			x		
Canberra S100 files	*.mca	x		x		X
Canberra binary spectrum files	*.cnf	x	x	x		
Canberra text spectrum files	*.lis			x		
Hyperlab	*.spe	X			X	x
IAEA spectrum files	*.k0s		x	X		
Nuclear Data Accuspec	*.nda			x		
Nucleus PCA	*.spm			x		
Ortec integer spectrum files	*.chn		x	x	x	x
Ortec spectrum files	*.spc		x	x		
Sampo spectrum files	*.spe	x		x		
Silena EMCAPlus	*.sip			x		
Silena	*.sil			x		
Peak area input formats						
IAEA peak area files	*.k0p			X		X
Canberra text spectrum analysis file	*.rpt	x		x		X
Canberra binary spectrum files	*.cnf	x		x		
Hyperlab	*.ptf	X				X
Hyperlab	*.csv				X	
Hypermet peak lists	*.pkl	x				
SAMPO peak analysis file	*.ptf	x		x		
GAMMAVISION text peak analysis file	*.gvt			x		
GAMMAVISION report file	*.rpt				x	
MAESTRO text peak analysis file	*.omt			x		

4. THE k_0 SOFTWARE INTERCOMPARISON

As the objective was to test the differences in the results obtained due to the differences between the participating codes, all other sources of possible variation were minimized. For that purpose, one set of experimental data was prepared, including all the quantities and information necessary for a full analysis with the different software packages, was prepared and provided to the participants. This included, for instance, data for efficiency calibration, irradiation facility characterization, and sample spectra, including all peak areas and energies. The data provided allowed the participants to employ different approaches to the characterization of the detector and of the irradiation facility.

It is clear that, had the participants implemented the k_0 method exactly as described in De Corte's thesis [23], including identical implementation of the methods there prescribed for characterization of the irradiation facility, efficiency curve modelling and efficiency conversion, they would have obtained exactly the same results (not considering very minor differences due to programming language and architecture of the computer system used). The uncertainties as reported by the codes, taking into account counting statistics and other sources of uncertainty, are less relevant for the differences in the results obtained between the codes, because most of those sources of variation were eliminated by the experimental design.

The use of a CRM as sample was one important element of the design of the intercomparison, because it allowed for a comparison between the results obtained by each code and the certified values. Discrepancies pointed to possible improvements in the codes. The uncertainties reported by each code are highly relevant for these considerations, because they determine whether a numerical difference is an actual discrepancy. The elements of interest were selected on excellent detectability and intended to target various aspects of k_0 -INAA, such as having only one gamma-ray energy or multiple, being visible in only one measurement or more, being subject to (threshold) interferences, suffering from true-coincidence summing, et cetera.

4.1. DATA

In this section the data used for the intercomparison is described.

4.1.1. Data for detector characterization

All experiments, including preparation of the samples, irradiation and counting, were done at the Jožef Stefan Institute (JSI), using its TRIGA Mark II research reactor. JSI participates in the IAEA proficiency testing by intercomparison exercises of NAA laboratories since 2011, demonstrating consistently very high performance [46, 47].

The spectra were acquired with a 40 % relative efficiency germanium detector in a vertical dipstick configuration. The point sources listed in Table 3 were counted at five different platform positions, corresponding to distances between the point source and the end cap of the detector of 203.4, 123.4, 83.4, 43.4 and 23.4 mm. Some of the point sources were measured only at the 203.4 mm reference position. Counting times were chosen to be sufficiently long to obtain expected counting statistics uncertainties of less than 0.1 % in the main peaks. Radionuclide data from Ref. [48] were used.

TABLE 3. CALIBRATION SOURCES AND DISTANCES FROM THE DETECTOR

Nuclide	Producer ^a	Ref. date	Activity (Bq)	Unc. % (k=2)	Distances
²⁴¹ Am	CMI	20/10/2014	2.008E+04	0.8	All
²⁴¹ Am	LMRI	15/06/1988 at 12:00	3.790E+04	2.0	All
¹⁰⁹ Cd	CMI	20/10/2014	4.140E+04	2.0	All
⁵⁷ Co	CMI	20/10/2014	5.008E+04	0.8	All
⁵⁴ Mn	CMI	20/10/2014	4.004E+04	2.0	All
⁶⁵ Zn	CMI	20/10/2014	3.753E+04	1.2	All
¹³⁷ Cs	LMRI	15/06/1988 at 12:00	3.972E+04	1.5	All
¹³³ Ba	PTB	01/09/1989	2.360E+05	1.5	203.4 mm
¹⁵² Eu	PTB	01/09/1989	2.160E+05	2.0	203.4 mm
²²⁶ Ra	PTB	01/09/1989	1.587E+05	2.81	203.4 mm
⁶⁰ Co	CMI	20/10/2014	2.319E+04	1.2	203.4 mm
¹⁹⁸ Au	JSI	30/06/2016 at 17:35:00	unknown	unknown	All

^a CMI: Czech Metrology Institute; LMRI: Laboratoire de métrologie des rayonnements ionisants, France; PTB: Physikalisch-Technische Bundesanstalt; JSI: Jožef Stefan Institute, Slovenia.

4.1.2. Data for characterization of the irradiation facility

The data needed to characterize the irradiation facility, i.e. to determine the k_0 parameters f and α , metal foils of pure Fe, Zn, Zr and an Al-Au alloy were stacked, irradiated simultaneously for 45 minutes and measured separately. Two irradiations were performed, one with 1 mm thick cadmium cover and one without ('bare'). Measurements were performed after waiting times ranging from about 8 hours to three days. Table 4 includes further information on the irradiations. Note that the distances between the sample and the detector end cap are not exactly the same as those for the reference point source data.

TABLE 4. FLUX MONITOR FOILS USED TO CHARACTERIZE THE IRRADIATION FACILITY

Foil material	Purity (%)	Radius (mm)	Height (mm)	Mass ("bare" irradiation) (g)	Mass (Cd-covered irradiation) (g)	Distance between sample and the detector end cap (mm)
Al-0.1% Au	0.1003 % Au	3.4	0.1	0.00934	0.00933	202
Fe	≥ 99.996	3.2	0.1	0.02475	0.02196	22
Zn	99.99+	3.5	0.025	0.00682	0.00693	122 and 22
Zr	99.8	3.0	0.14	0.02542	0.02507	202 and 22

4.1.3. Flux monitor and sample spectra

The sample chosen for the intercomparison was the CRM BCR-320R, a channel sediment [49] with 16 elements certified with stated uncertainties ranging from 2.5 to 6% (for a coverage factor $k=1$), and two further elements with indicative values. 11 out of the 16 certified elements (with uncertainties ranging from 2.5 to 5.3% for a coverage factor $k=1$), and an additional six

elements not mentioned in the certificate but reported by all the participants, were used for the purposes of this intercomparison.

Two samples of this CRM were prepared by filling cylindrical polyethylene capsules with internal radius and height of 4 mm and 4 mm, respectively. The determination of the moisture correction factor followed the prescription of the CRM's certificate — oven-drying at least 1 gram of not-to-be-analysed material at 105 °C until constant mass is attained. A 1.14968 gram initial mass was used, yielding a correction factor of 0.9744. One sample was irradiated on top of an Al-Au alloy flux monitor for 30 seconds. The other sample was put together with three dummy samples, sandwiched between three flux monitors (see Figure 19), and irradiated for 12 hours in the same facility and position. Details of the sample and flux monitors used, irradiation times and counting positions are given in Table 5. A blank was not included. Instead, information on the blank composition was provided to all participants, only affecting the results for Cr.

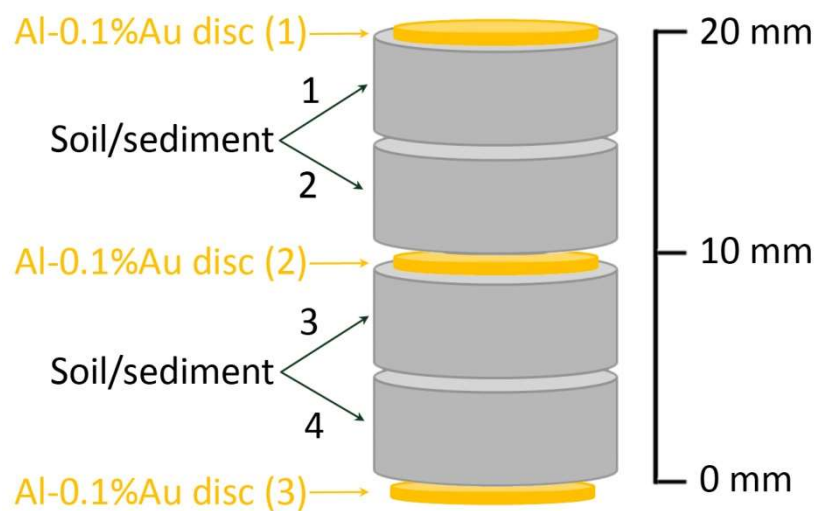


FIG. 19. Sample and flux monitor configuration during irradiation. The spectra of soil/sediment (CRM BCR-320R) sample #4 were used in the intercomparison, as well as the spectra of the three flux monitors.

TABLE 5: SAMPLE AND FLUX MONITOR DETAILS

Sample	Radius (mm)	Height (mm)	Measured mass (g)	Dry mass used (g)	Irradiation time	Sample-detector distances and approximate waiting times
BCR-320R	4.0	4.0	0.20766	0.20234	30 s	202 mm (8 min), 202 mm (39 min)
Al-0.1%Au	3.4	0.1	0.00951	Au: 9.539 µg	30 s	82 mm (6 hours)
BCR-320R	4.0	4.0	0.19343	0.18847	12 hours	202 mm (4 days), 22 mm (9 and 27 days)
Al-0.1%Au	3.4	0.1	0.00933	Au: 9.358 µg	12 hours	at 202 mm (6 days)
Al-0.1%Au	3.4	0.1	0.00915	Au: 9.177 µg	12 hours	202 mm (6 days)
Al-0.1%Au	3.4	0.1	0.00930	Au: 9.328 µg	12 hours	202 mm (6 days)

4.1.4. Peak areas

The peak areas and energies were determined from the raw spectra by JSI using Hyperlab 2014 [31]. They were included in the set of data made available to the participants, in addition to the raw spectra. According to the intercomparison definition, the raw spectra were to be used exclusively for detection limit estimation. This means that only the calculation core of the codes, that processes peak areas for given energies, was tested in the intercomparison. Several codes have algorithms to extract the peak areas and energies, and, when used, these may lead to additional differences in the results.

4.2. INTERCOMPARISON PROCEDURE

4.2.1. First round

In the first round of the software intercomparison, the spectra, peak areas and energies, and experimental data were provided to the participants, including indicative data on the matrix composition. The information that the CRM used was the BCR-320R, and that the two samples were of the same material, was withheld from the participants. The participants were requested to report on preselected elements and peaks. The elements and peaks to be reported on by the participants were selected taking into account that induced radionuclides could be typically detected in a sediment sample via short or long irradiation including a wide energy interval of gamma rays (from 100 keV to 3000 keV). High counting statistics for the peaks involved were required, in order to allow for testing the propagation of other sources of uncertainty to the results. Certified mass fractions of some elements in the sample were required in order to check the accuracy of the data reported. Last but not least, elements were selected to address known complexities of the k_0 -method, such as the necessity to correct for coincidence summing, or to correct for spectral and primary interferences.

As part of the intercomparison, the participants provided information on the nuclear data and k_0 constants that they used. The results were reported for different data analysis procedures: results obtained from single peaks; from all the peaks within one single spectrum; and from all the spectra combined. The results were submitted by the participants to the data provider (JSI).

Two outliers were identified on the first submission. As these were trivial errors not related to the software itself, the participants in question could correct their reports before processing the data. In one case, the $^{27}\text{Al}(n,p)^{27}\text{Mg}$ reaction contribution had not been corrected for. Another participant had entered a wrong irradiation time for the flux monitors. Finally, one participant (k0-DALAT) could not use the peak areas provided, and determined them within the code, as this is the normal way to operate this code and there is no option to use externally provided peak areas.

4.2.2. Second round

After the first round, the identity of the reference material was revealed to the participants. The participants were then asked to investigate the causes of differences between the results obtained for those elements that are certified, and to improve their software if it was found out that the differences could be assigned to some particular calculation step. The results obtained by each participant for the efficiency curves were shared and compared. After software improvements were made, the participants submit the second round of results, and provided further details on the intermediate computational steps.

The improvements made to the various software packages are the following:

KayWin

- None.

k0-DALAT

- The fourth-order efficiency curve was better fitted at energies above 1408 keV, using the ^{24}Na peaks;
- The correction for the Hg-Se interference at 279 keV was done;
- The peak areas distributed to the participants were used;

Additionally, a more experienced user decided which individual peaks and spectra were used for each element.

k0-IAEA

- The method for peak-to-total detector characterization was improved, to include the peak area in the ‘total’;
- The k_0 data used were according to the k_0 database, leading to minor changes in a few k_0 constants and half-lives.

k0-INRIM

- The measurement equation was improved with parameters modelling the gamma self-absorption correction, the gamma interference correction, the moisture correction, and the non-linearity of the gamma efficiency with the detector distance;
- The possibility for manual interference correction performed by the user was introduced and employed;
- The neutron flux characterisation was improved, with quantification of the fast neutron flux.

k0-IPEN

- Correction due to spectral interferences was implemented;
- The k_0 data were adjusted according to the k0 database;
- Manual correction of the threshold reactions interferences was made;
- The values for f and α were adjusted due to correction of the efficiencies relative to the reference position.

4.2.3. Efficiency curves

Relative efficiencies, that is, the ratio of detection efficiencies for the sample and flux monitor at each given energy, matter most in the k_0 -NAA method. The participants were asked to report the absolute efficiencies they calculated for all the peaks used in the analysis, for the reference counting geometry and for the sample and flux monitor counting geometries that were actually used. The ratios of efficiencies, which are used in the concentration calculations, were calculated from the absolute efficiencies to enable comparison of the efficiencies used by all the participants. This is a critical quantity, as it is directly reflected in the final results for the elemental amounts. The efficiency ratios for the sample at 202 mm versus the flux monitor at 82 mm are used to calculate the mass fractions for the short irradiation data. For the long irradiation, it is the efficiency ratios for the sample at 202 mm and 22 mm with respect to those for the flux monitor at 202 mm that are needed.

4.2.3.1. Conversion of detection efficiencies

Most participants converted the detection efficiencies from the reference counting geometry to the actual sample counting geometry using the following computational methods.

- k0-DALAT; a fourth-order polynomial was fitted to the available data points.
- k0-IAEA: The peak-to-total calibration was obtained from the ^{137}Cs source measured at 23.4 mm from the end cap, and the full energy peak efficiency curve was calculated from the ^{152}Eu spectrum measured at 203.4 mm. Monte Carlo methods were used to calculate the efficiency conversion, to a 0.1 % statistical precision.
- k0-INRIM: A sixth-order polynomial was fitted to all the data available for the reference position, that is, including all the gamma lines observed in all the sources measured. For the other counting geometries, the efficiency curves were obtained by calculating the count rate ratios of coincidence-free gamma lines with respect to the reference position; then, the obtained ratios were fitted with similar sixth-order exponential polynomial equations. In the cases where the non-reference counting geometries do not coincide with the actual sample counting geometries, vertical efficiency corrections were done by modelling an inverse square trend, which also evaluated from the count rate ratio data.
- k0-IPEN: All available spectra and data points, from 53 keV up to 2000 keV, were used for the full energy peak efficiency calibration at the reference position. For the high energy (2754 keV) ^{24}Na gamma line, a Monte Carlo method was used. All available mono-energetic spectra were used to determine the peak-to-total efficiency curve.
- KayWin: The SOLCOI [3] routine is used for efficiency conversion. SOLCOI is a combination of SOLANGE [2] with the coincidence correction software COINCALC [41].

The mass fractions are determined mainly by the relative efficiencies. The absolute efficiencies can have a second order effect on the mass fractions through the corrections for true coincidence summing. coincidence correction factors for all peaks were tabulated in order to be able to compare the codes in this respect.

4.2.3.2. Neutron flux parameters

All codes except KayWin used the ‘triple bare’ method for the determination of the k_0 parameters f and α . KayWin used the ‘Cd-cover’ method. The fast flux was determined by all the participants using the $^{27}\text{Al}(n,\alpha)^{24}\text{Na}$ and/or the $^{54}\text{Fe}(n,p)^{54}\text{Mn}$ reactions.

4.3. RESULTS

In this section the results obtained in the first of second rounds of the intercomparison exercise are presented.

4.3.1. First round

For each element, the ratio of the single reported mass fraction to the unweighted average of all reported mass fractions was calculated. The results are shown in Figure 20. The variation due to code differences is computed as the standard deviation of these ratios. The observed overall variation is 6.4 %, while the observed variation for certified and uncertified elements is 5.6 % and 7.9 %. If outliers Hg and Mg would be excluded, the overall variation would drop to 3.6 %.

For each certified element, the ratio of the reported mass fraction to the certified value was calculated. The resulting ratios are shown in Figure 21.

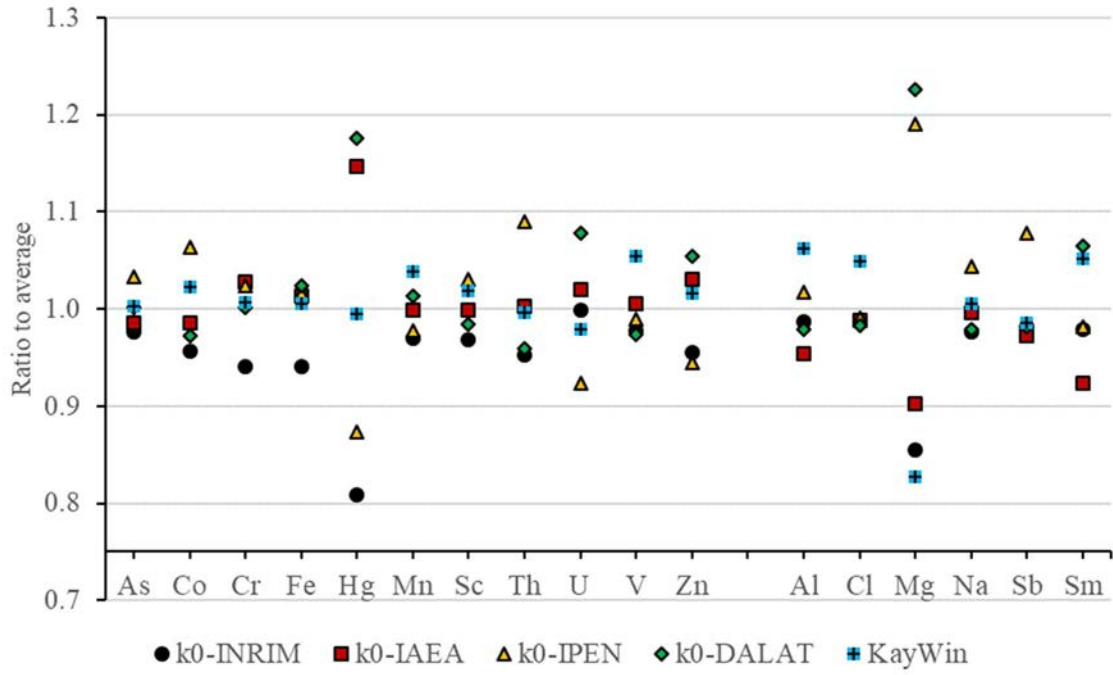


FIG. 20. Ratio between the mass fractions (as reported in the first round) and the average of all codes for that element. Elements As through Zn were certified, Al through Sm were not.

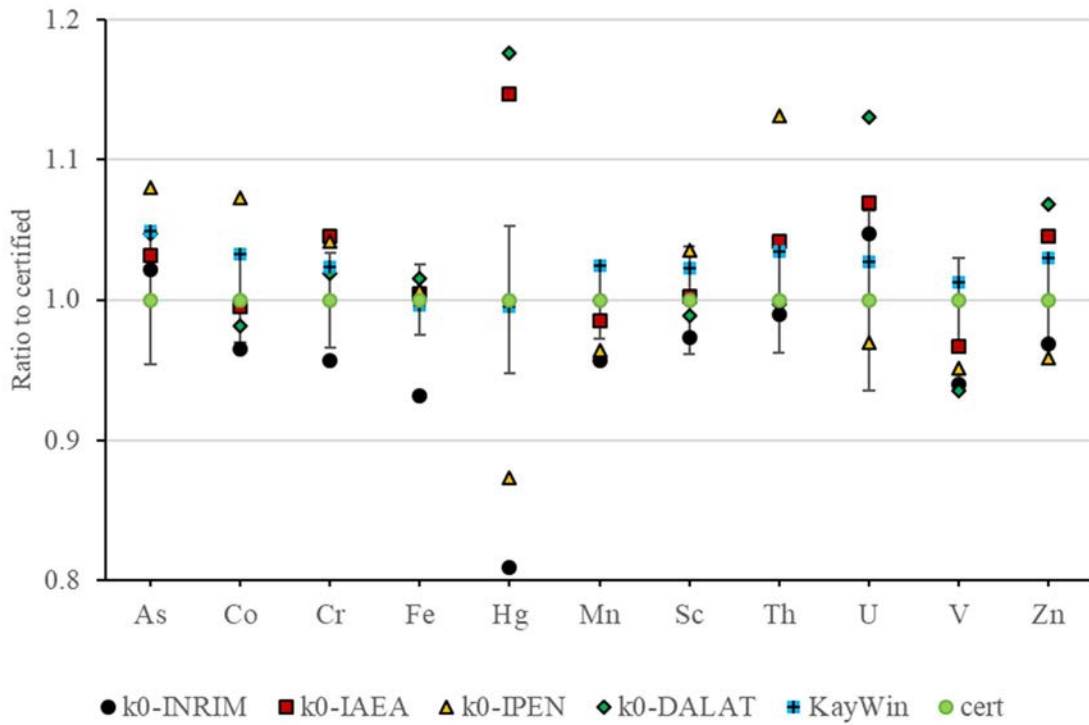


FIG. 21. Ratio between the mass fractions (as reported in the first round) and the certified value for that element. The error bars indicate the $k=1$ uncertainty in the certified values.

The overall quality of the results of each code was assessed with the aid of a Q^2 score, defined as

$$Q_j^2 = \frac{1}{N} \sum_{i=1}^N \frac{(c_{ij} - c_{ci})^2}{s_{ci}^2} \quad (35)$$

where

N is the number of mass fractions reported

c_{ij} is the mass fraction reported for element i by code j

c_{ci} is the certified mass fraction and

s_{ci} is the 1 standard deviation uncertainty in the certified mass fraction.

The uncertified mass fractions are not used for the calculation of the Q^2 score. The lower the Q^2 score, the better the overall agreement with the certified values. One should note that outliers strongly Q^2 score affect the value. They were not removed, because they indicate that systematic errors may be present. A value of the Q^2 score below 1 should not be achievable, because it would mean that the results obtained have a better precision than what is warranted by the uncertainties given in the CRM certificate. Indeed, whatever the analysis method used, it should introduce an additional contribution to the uncertainty, not accounted for in the Q^2 calculation. All in all, a Q^2 score equal to 1 indicates that the software package used did not introduce a significant extra uncertainty.

A reduced χ_r^2 score was used as a measure of the statistical control of each code (statistical control being, in this context, the ability of the code to report appropriate inaccuracies in mass fractions). It was defined as:

$$\chi_{rj}^2 = \frac{1}{N} \sum_{i=1}^N \eta_{ij}^2 \quad (36)$$

where the η_{ij} are the zeta scores for each mass fraction, defined by

$$\eta_{ij} = \frac{c_{ij} - c_{ci}}{\sqrt{s_{ij}^2 + s_{ci}^2}} \quad (37)$$

and s_{ij} is the 1 standard deviation uncertainty for the mass fraction i reported by code j .

The zeta scores are a measure of the agreement of the result obtained by each code with the certified values for each element, taking the uncertainty reported by the code into account. They are shown in Figure 22 for the first round of reported results.

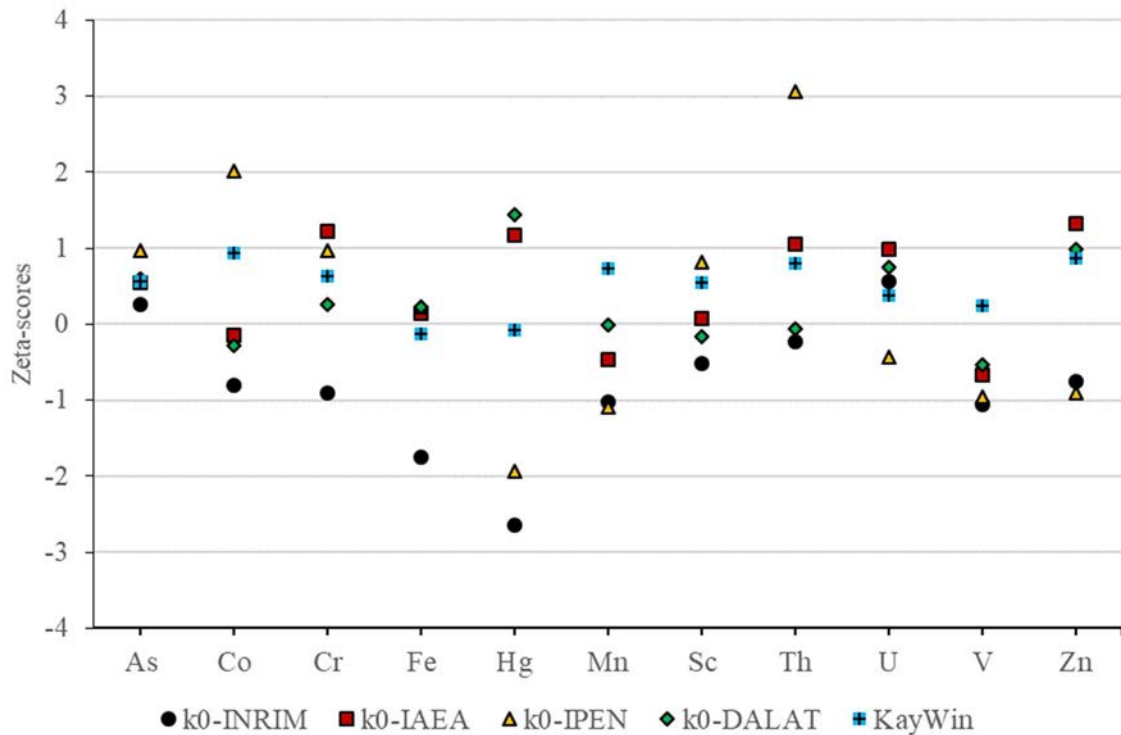


FIG. 22. Zeta-scores for the certified elements in the first round.

Considering 11 degrees of freedom corresponding to the 11 certified elements used, the χ_r^2 scores are expected to range between 0.35 and 2 for a code to be in control with 95% confidence. A score below 0.35 or above 2 indicates that an overestimation or an underestimation of the combined uncertainty may have been evaluated by the code, respectively. The calculated resulting Q^2 scores and χ_r^2 scores are given in Table 6 for all the participating codes.

TABLE 6. Q^2 AND χ_r^2 SCORES FOR THE PARTICIPATING CODES (FIRST ROUND)

Code name	Q^2	χ_r^2
k0-INRIM	2.91	1.35
k0-IAEA	1.45	0.69
k0-IPEN	3.22	2.07
k0-DALAT	2.43	0.41
KayWin	0.55	0.37

4.3.2. Second round

A similar procedure as in the first round was adopted for the second round. For each element, the ratio between the reported mass fraction and the unweighted average of the mass fractions reported by all the codes was calculated, shown in Figure 23. The standard deviation calculated for all elements and all codes is 3.0%. For the certified and uncertified elements it is 2.7% and 3.4%, respectively.

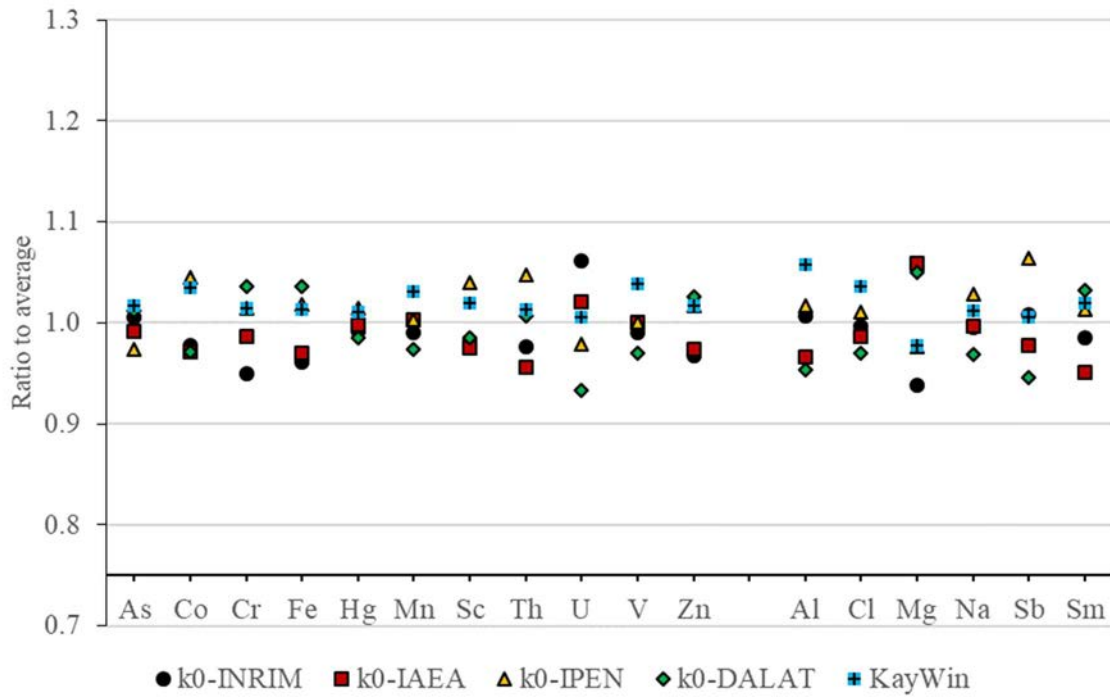


FIG. 23. Ratio between the mass fractions (as reported in the second round), and the average of all codes for that element. Elements As through Zn were certified, Al through Sm were not.

For each participant, the average and standard deviation of the ratio to average values shown in Figure 23 was calculated for three different groups of results: first, for the results calculated using both short and long irradiations; and then, for the results calculated using only either the short or the long irradiation. The results are shown in Table 7, where some systematic biases can be observed. The reduced chisqr of these biases amounts to 7.1.

TABLE 7. AVERAGE AND STANDARD DEVIATION (STD) OF THE RATIO TO AVERAGE VALUES

	k0-DALAT		k0-IAEA		k0-INRIM		k0-IPEN		KayWin	
	average	STD	average	STD	average	STD	average	STD	average	STD
Short and long irradiations	0.991	0.009	0.987	0.006	0.987	0.007	1.015	0.006	1.019	0.004
Short irradiation	0.984	0.017	1.003	0.015	0.984	0.012	1.001	0.007	1.028	0.013
Long irradiation	0.991	0.009	0.984	0.005	0.988	0.007	1.018	0.007	1.018	0.003

The ratios between the reported mass fractions and the certified values were calculated for the 2nd round. The resulting ratios are shown in Figure 24.

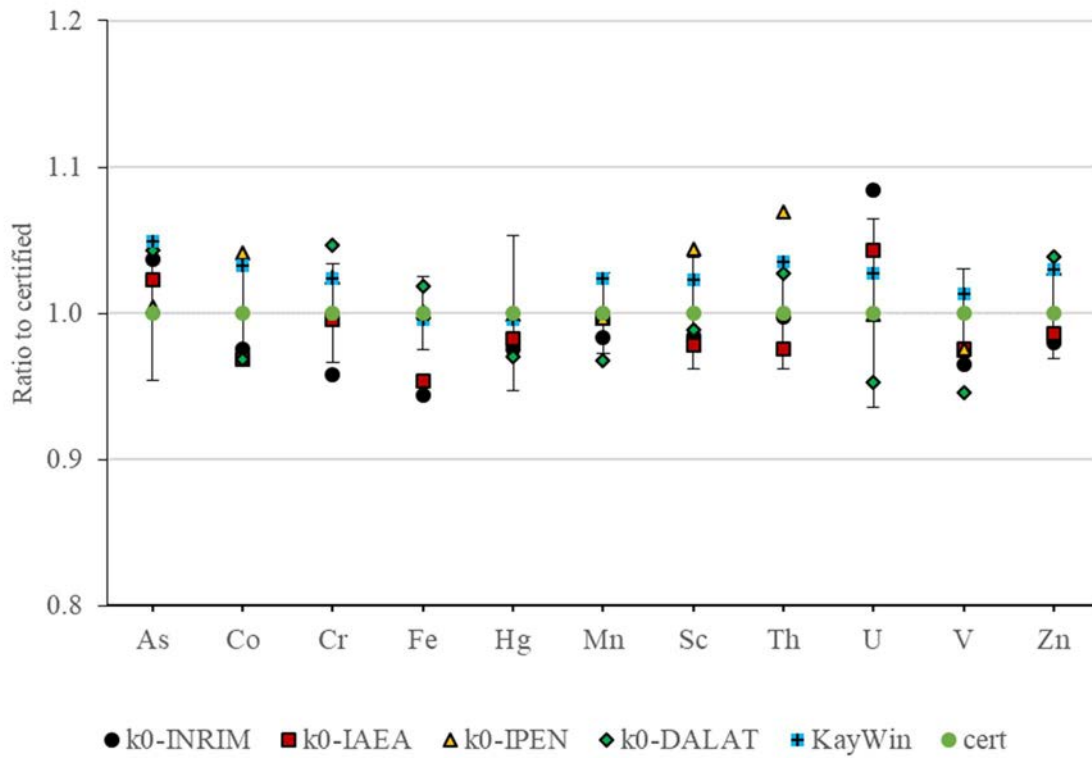


FIG. 24. Ratio between the mass fractions (as reported in the second round) and the certified value for that element. The error bars indicate the $k=1$ uncertainty in the certified values.

The zeta-scores for the second round are shown in Figure 25.

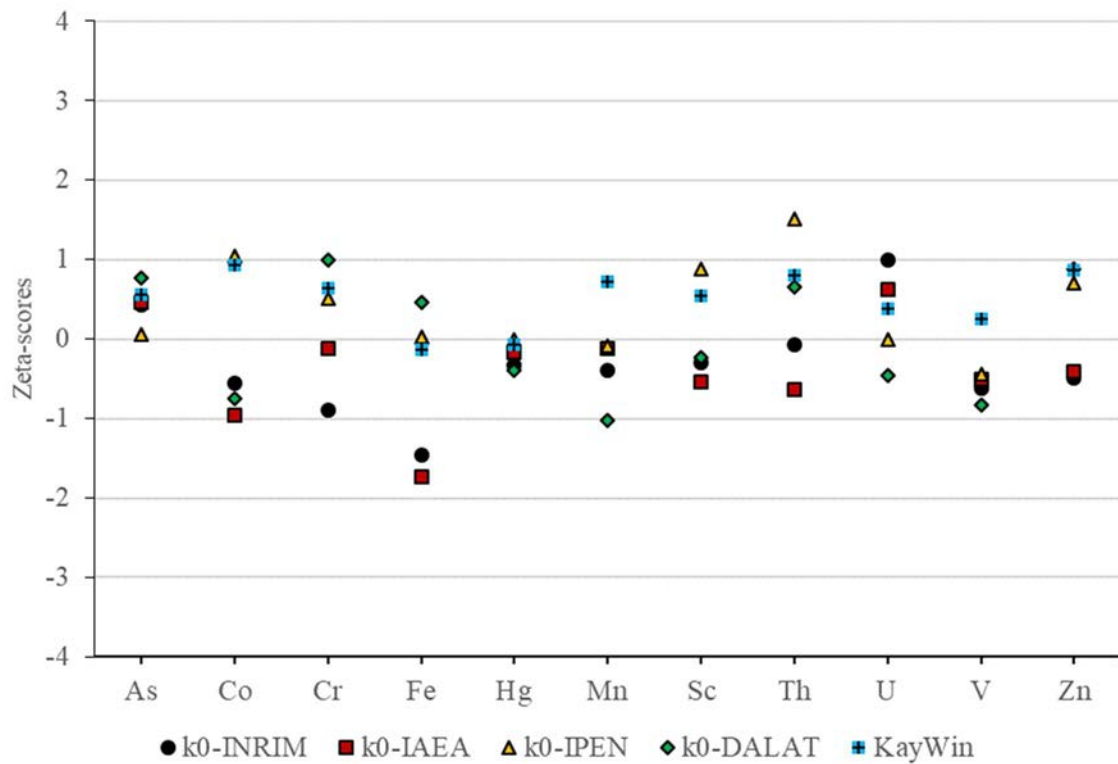


FIG. 25. Zeta-scores for the certified elements in the second round.

The Q^2 scores and χ_r^2 scores obtained in the second round are shown in Table 8 for all the participating codes.

TABLE 8. Q^2 AND χ_r^2 SCORES FOR THE PARTICIPATING CODES (SECOND ROUND)

Code name	Q^2	χ_r^2
k0-INRIM	1.13	0.49
k0-IAEA	0.66	0.52
k0-IPEN	0.86	0.46
k0-DALAT	1.10	0.51
KayWin	0.49	0.37

4.3.3. Efficiency curves and true coincidence summing

Consider the detection probability efficiency for a given gamma ray peak at a certain energy, corresponding to a certain element, observed in the sample spectrum. The mass fraction of that element calculated with the k_0 method is proportional to the inverse ratio between that efficiency and the detector efficiency for the 411 keV peak of ^{198}Au from the flux monitor. For each such ratio, the value obtained by each participant was divided by the average of all participants. The results are shown for the different combinations of sample and flux monitor positions used: in Fig. 26 for the sample at 202 mm with the flux monitor at 82 mm, in Fig. 27 for the sample and flux monitor both at 202 mm, and in Fig. 28 for the sample at 22 mm and the flux monitor at 202 mm.

The standard deviation of these ratios of efficiency ratios is 2.1%, 1.9% and 3. % for the three cases, respectively.

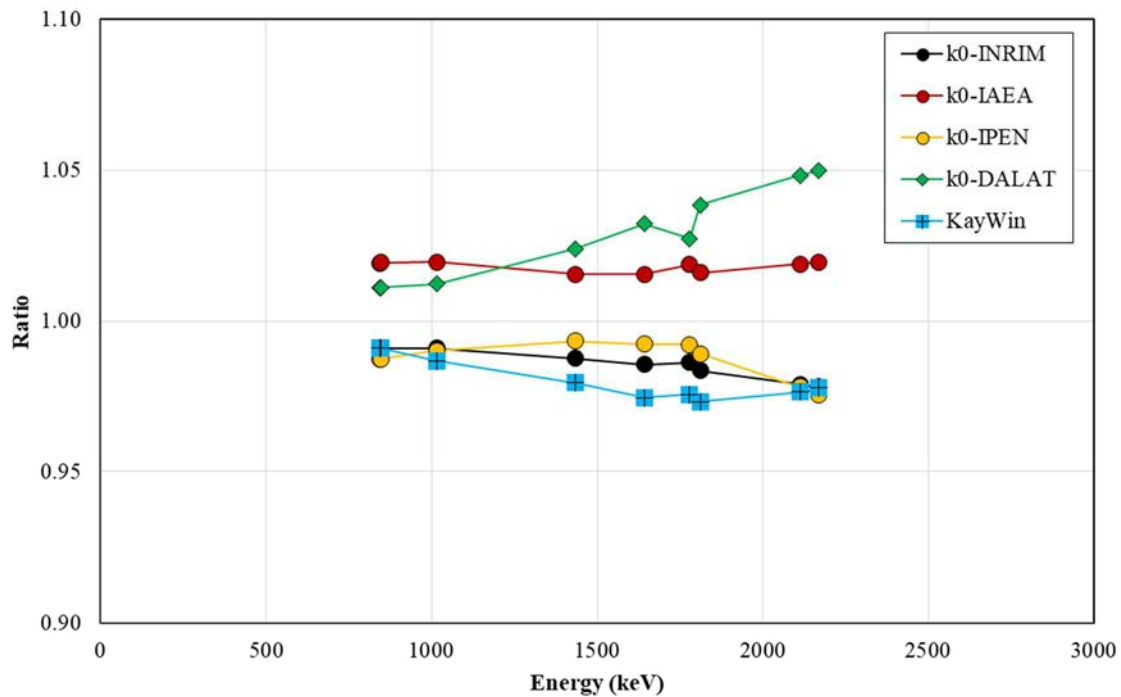


FIG. 26. Code-specific efficiency ratios, normalized to the average over all codes, for sample peaks measured at 202 mm versus the flux monitor 411 keV peak measured at 82 mm.

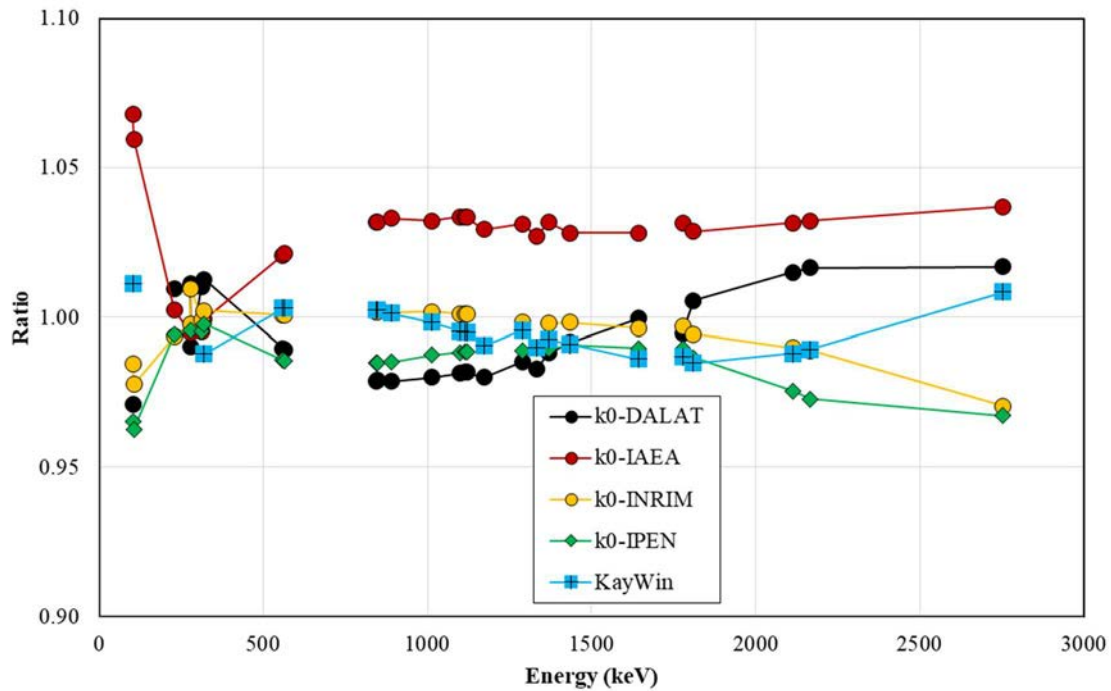


FIG. 27. Code-specific efficiency ratios, normalized to the average over all codes, for sample peaks measured at 202 mm versus the flux monitor 411 keV peak measured at 202 mm.

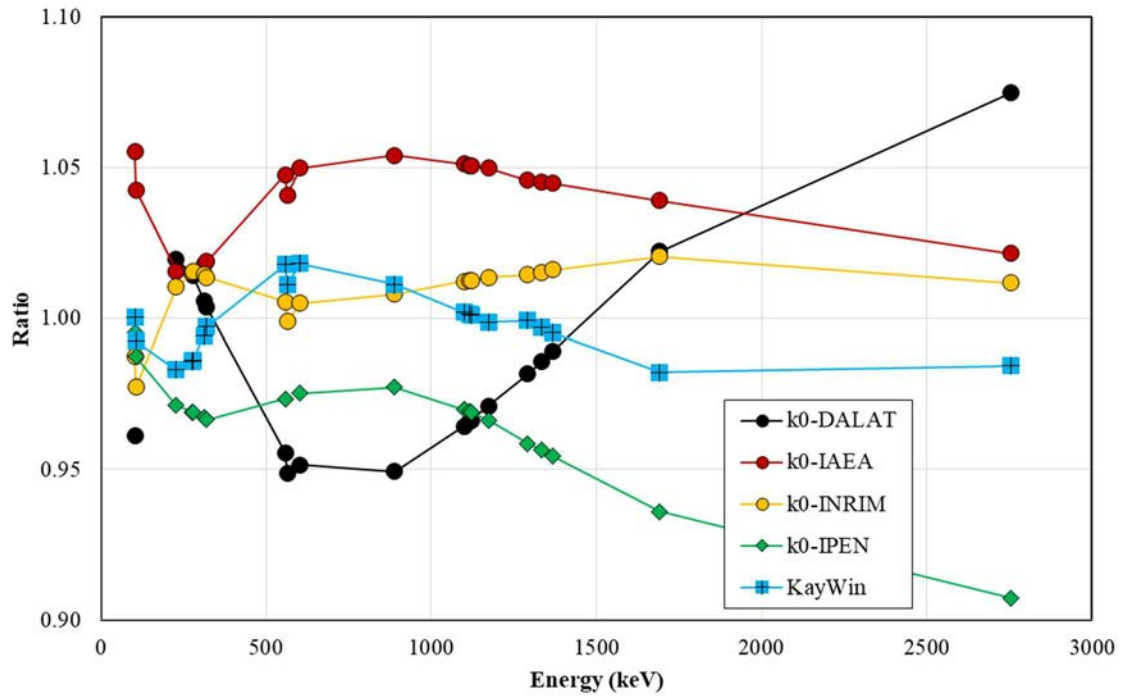


FIG. 28. Code-specific efficiency ratios, normalized to the average over all codes, for sample peaks measured at 22 mm versus the flux monitor 411 keV peak measured at 202 mm.

True coincidence summing correction factors for selected peaks are shown in Fig. 29. The overall variation observed after dividing each correction factor by the average for that peak energy was found to be 0.4%.

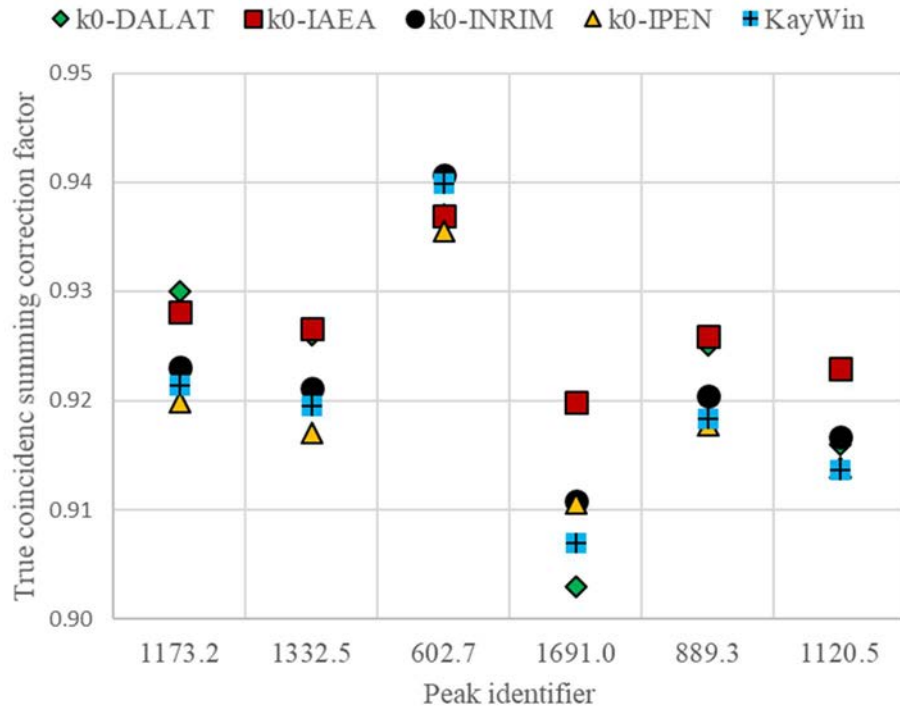


FIG. 29. True coincidence summing correction factors reported by the participants for the nuclides, peaks and counting geometry where coincidence summing has the largest effect: 1173 and 1332 keV of ^{60}Co , 603 and 1691 keV of ^{124}Sb , and 889 and 1120 keV of ^{46}Sc , all at 22 mm from the end cap of the detector).

4.3.4. Neutron spectrum parameters

The participants used the efficiency curves as determined by them, together with the spectra provided, to determine the conventional subcadmium flux ϕ_0 , the k_0 parameters f and α , as well as the fast neutron flux for the irradiation position used. The results obtained in the 2nd round are given in Table 9. More significant digits than usual are shown as, although all of the codes used the same input data, propagated counting statistics and other sources of uncertainty can affect the results; this is illustrated by the standard deviation (columns STD).

TABLE 9. REPORTED NEUTRON SPECTRUM PARAMETERS

code	method	ϕ_0		f		alpha		fast flux	
		$\text{cm}^{-2}\text{s}^{-1}$	STD	n/a	STD	n/a	STD	$\text{cm}^{-2}\text{s}^{-1}$	STD
k0-DALAT	bare, Fe	1.067E+12	7.4E+10	26.50	5.30	0.012	0.005	1.910E+11	9.5E+09
k0-IAEA	bare, Fe	1.092E+12	4.0E+09	26.49	1.05	0.017	0.007	1.369E+11	3.0E+09
k0-INRIM	bare, Fe	1.120E+12	3.7E+10	30.25	2.61	-0.006	0.014	1.293E+11	4.2E+09
k0-IPEN	bare, Al	1.093E+12	1.5E+10	29.06	1.30	-0.009	0.004	1.410E+11	1.9E+10
KayWin	Cd-ratio, Fe	1.072E+12	1.0E+10	26.80	0.80	0.000	0.010	1.420E+11	1.4E+09
KayWin ^a	bare, Fe	-	-	30.46	n/a	-0.009	n/a	-	-

^aThe KayWin bare data is given for information only, as it was not used in other calculations.

4.4. DISCUSSION OF THE RESULTS OBTAINED

In this section the results obtained in the first of second rounds of the intercomparison exercise are discussed.

4.4.1. Mass fractions

The results of the participating codes are in reasonably good agreement in the first round of results, and improve in the second round. The differences between the codes can be explained to a great extent by the differences in the efficiency curves and the resulting efficiency ratios shown in Figures 26–28, used to determine the neutron flux parameters and the mass fractions. The procedure selected for the determination of the neutron spectrum parameters (e.g. ‘bare’ or Cd-cover methods) also contributes to the difference observed.

The results for Hg and Mg in the first round of reporting displayed a dispersion between the codes significantly higher than observed for the other elements (see Fig.20). The 279 keV Hg peak strongly interferes with the ^{75}Se peak at the same energy, the latter suffering from strong coincidence summing effects. The Mg peak includes a strong contribution from the $^{27}\text{Al}(n,p)^{27}\text{Mg}$ reaction. The other elements used in this intercomparison exercise were relatively simple to analyse, as they were essentially free from interferences. This can be seen in the small differences in the results obtained already in the first round.

As the dispersion in the Mg mass fractions observed in the first round was likely due to interference effects, the participants were asked to report the threshold capture cross sections that they had used. These included not only the $^{27}\text{Al}(n,p)^{27}\text{Mg}$ reaction, but also $^{54}\text{Fe}(n,p)^{54}\text{Mn}$ and $^{27}\text{Al}(n,\alpha)^{24}\text{Na}$, which were used by some participants to establish the fast neutron flux in the procedure to characterize the irradiation facility.

The cross-section data used by the different participants are shown in Table 10. It is concluded that the observed variation in the threshold capture reactions and respective cross sections used explains, to a large degree, the remaining dispersion in the Mg results.

The Q^2 score for the KayWin results in the first round, and those for KayWin and k0-IAEA in the second round, are below unity. This finding could possibly originate from the k_0 -NAA method having been used for the certification of the BCR-320R CRM, leading to a correlation between the certified mass fractions and those determined in present intercomparison exercise. However, the detailed certification report [49] shows that k_0 -NAA was one out of 13 techniques employed in the certification (including INAA and radiochemical NAA, which would not lead to results correlated with those obtained with k_0 -NAA), and only one laboratory out of 16 used k_0 -NAA. The k_0 -NAA results contributed to the certification of As, Co, Cr, Fe, Sc, Th and Zn; seven out of 11 certified elements used in this intercomparison. However, the certification of each of these seven elements used results from between seven and 11 other laboratories that employed different techniques. Therefore, a significant correlation between the certification process and the low Q^2 scores determined for KayWin and k0-IAEA can be excluded. Therefore, overestimation of the certified mass fraction uncertainties in these two codes is the more likely cause for the observation. The χ_r^2 values are lower than the Q^2 values in all cases, which is inevitable given that the uncertainty estimates of the participating codes themselves are also included. All codes showed good statistical control at the 95% confidence level in both rounds.

As mentioned above, the certified mass fractions in the CRM used were certified with uncertainties ranging from 2.5 to 5.3% for a coverage factor $k=1$. These are not sufficiently

small to allow the extraction of definite conclusions on the inherent uncertainties associated with the k_0 -NAA method, besides the fact that these inherent uncertainties are better than a few %.

The results obtained in the second round by some of the participating codes improved markedly with respect to those of the first round. This was due to improvements in the codes, update of the k_0 data used to match the current k_0 database, interference corrections included or improved, correction of the efficiency values relative to the reference position, use of the distributed peak areas and not those internally calculated, and quantification of the fast flux not done in the first round. Some of these improvements led to a correction of all reported mass fractions, while others only impacted specific mass fractions. All improvements were made after the identity of the CRM used had been revealed and the results from all participants had been shared, as well as after fruitful discussions among the participants.

TABLE 10. NEUTRON CAPTURE CROSS SECTIONS FOR THE SPECIFIED THRESHOLD REACTIONS

code name	$^{27}\text{Al}(n,p)^{27}\text{Mg}$ (mbarn)	$^{54}\text{Fe}(n,p)^{54}\text{Mn}$ (mbarn)	$^{27}\text{Al}(n,\alpha)^{24}\text{Na}$ (mbarn)
k0-INRIM	3.84	81.7	0.699 *
k0-IAEA	3.9	79.2	1.18 *
k0-IPEN	4.2085	^a	0.725
k0-DALAT	4.0	82.5	0.725 *
KayWin	4.0	82.5	0.725 *

^a Not used.

4.4.2. Neutron spectrum parameters

The influence of the observed differences in reported f and α values in the mass fraction values obtained was assessed by calculating the neutron flux component $(f+Q_0(\alpha))_m/(f+Q_0(\alpha))_a$, where m and a refer to the flux monitor and analyte elements ($g(T)$, g_{th} and g_{epi} were all practically unity for all participants). This ratio accounts for the influence of the neutron spectrum on the mass fraction values calculated by the participants. It was calculated for each relevant activation reaction for the f and α values determined and used by each of the participants, and the results are shown in Table 11.

The neutron flux component values, normalized to the average of the values obtained by all the participants, is shown in Fig. 30. They are a measure of the impact of the different neutron spectrum parameters used on the reported mass fractions. The smallest impact in terms of relative variation is obtained for Sm (about 0.2%), while the highest is observed for U (4.3%).

In order to eliminate the impact in the calculated mass fractions of the dispersion in the f and α parameters, the mass fractions reported in the second round were divided by the correction factors given in Fig. 30. The dispersion in the mass fractions thus calculated, shown in Fig 31, is 3.0% overall (i.e. for all the elements), 2.7% for the certified elements and 3.5% for the uncertified elements. This compares to the values obtained before this correction was done, which were 3.0%, 2.7% and 3.4%, respectively. so no improvement was observed. Figure 30 does illustrate the fact that if f and/or α are off, the use of a high-Q flux monitor reaction such as $^{197}\text{Au} \rightarrow ^{198}\text{Au}$ will systematically impact all mass fractions determined through low-Q reactions, which is the majority. A low-Q reaction as flux monitor could be used instead, in practice, to reduce this impact on low-Q-based results. For each participant, the average and

standard deviation of the ratio to average values shown in Fig. 31 was calculated, and the results are shown in Table 12.

Comparing Fig. 31 to Fig. 23, it can be observed that the impact of this compensation of the effect of the dispersion in f , α values has an effect in the data for some elements, such as uranium, which exhibit a smaller dispersion after the correction is made.

TABLE 11. NEUTRON FLUX COMPONENT VALUES FOR ALL PAIRS OF f , α AND ACTIVATION REACTIONS USED

	k0-INRIM	k0-IAEA	k0-IPEN	k0-Dalat	KayWin	Average	STD
f	30.25	26.49	29.06	26.5	26.8	27.8	1.7
α	-0.006	0.017	-0.009	0.012	0	0.003	0.011
Certified elements							
As	1.0426	1.0681	1.0411	1.0636	1.0520	1.053	0.012
Co	1.4279	1.4723	1.4458	1.4748	1.4761	1.459	0.022
Cr	1.4977	1.5461	1.5202	1.5503	1.5551	1.534	0.024
Fe	1.4756	1.5233	1.4965	1.5269	1.5302	1.511	0.024
Hg	1.4801	1.5285	1.5013	1.5321	1.5354	1.516	0.024
Mn	1.4718	1.5193	1.4925	1.5228	1.5259	1.506	0.023
Sc	1.5029	1.5510	1.5258	1.5555	1.5608	1.539	0.024
Th	1.0973	1.1204	1.0985	1.1175	1.1097	1.109	0.011
U	0.3405	0.3338	0.3331	0.3312	0.3264	0.333	0.005
V	1.4967	1.5451	1.5191	1.5493	1.5539	1.533	0.024
Zn	1.4306	1.4799	1.4480	1.4815	1.4804	1.464	0.023
Uncertified elements							
Al	1.4885	1.5374	1.5102	1.5412	1.5449	1.524	0.024
Cl	1.4895	1.5383	1.5113	1.5422	1.5460	1.525	0.024
Mg	1.4919	1.5413	1.5138	1.5451	1.5488	1.528	0.025
Na	1.4947	1.5430	1.5170	1.5472	1.5517	1.531	0.024
Sb	0.7733	0.7770	0.7663	0.7730	0.7644	0.771	0.005
Sm	1.0285	1.0336	1.0290	1.0331	1.0316	1.031	0.002

TABLE 12. AVERAGE AND STANDARD DEVIATION (STD) OF THE RATIO TO AVERAGE VALUES, AFTER f , α CORRECTION

	k0-DALAT		k0-IAEA		k0-INRIM		k0-IPEN		KayWin	
	Average	STD	Average	STD	Average	STD	Average	STD	Average	STD
Short and long irradiations	0.983	0.008	0.979	0.006	1.003	0.005	1.024	0.006	1.011	0.004
Short irradiation	0.973	0.017	0.995	0.015	1.008	0.012	1.011	0.007	1.014	0.013
Long irradiation	0.983	0.008	0.976	0.005	1.003	0.005	1.027	0.007	1.012	0.003

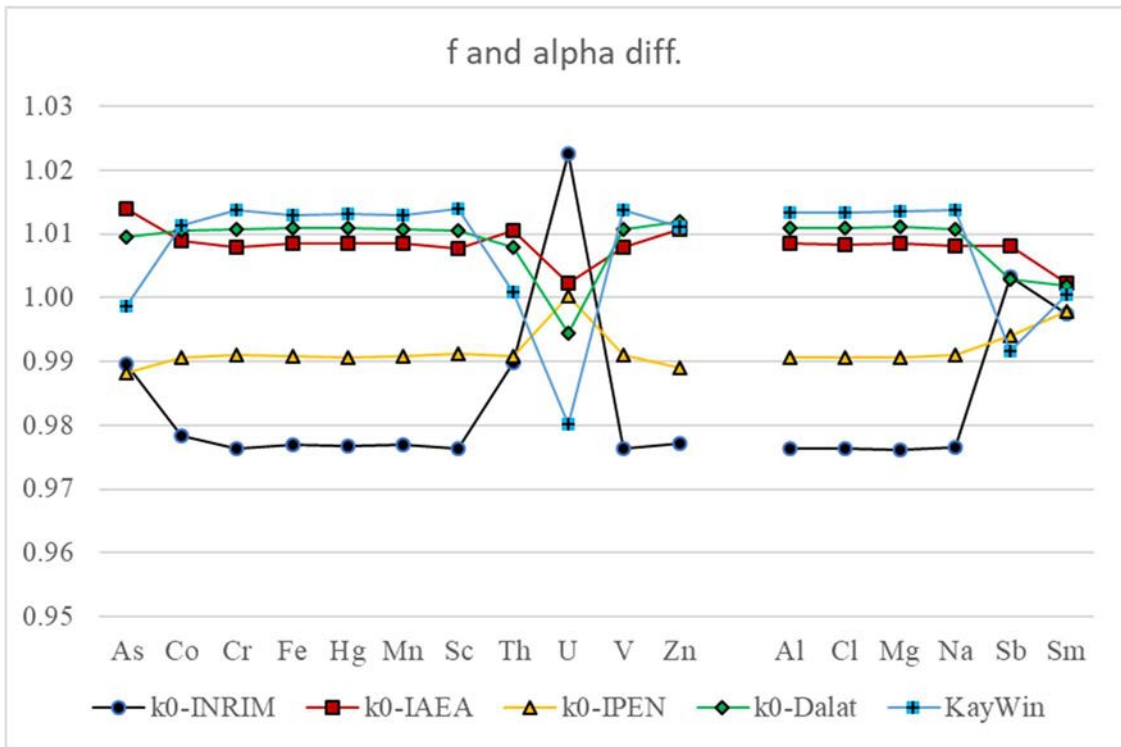


FIG. 30. Neutron flux component normalized to the average value.

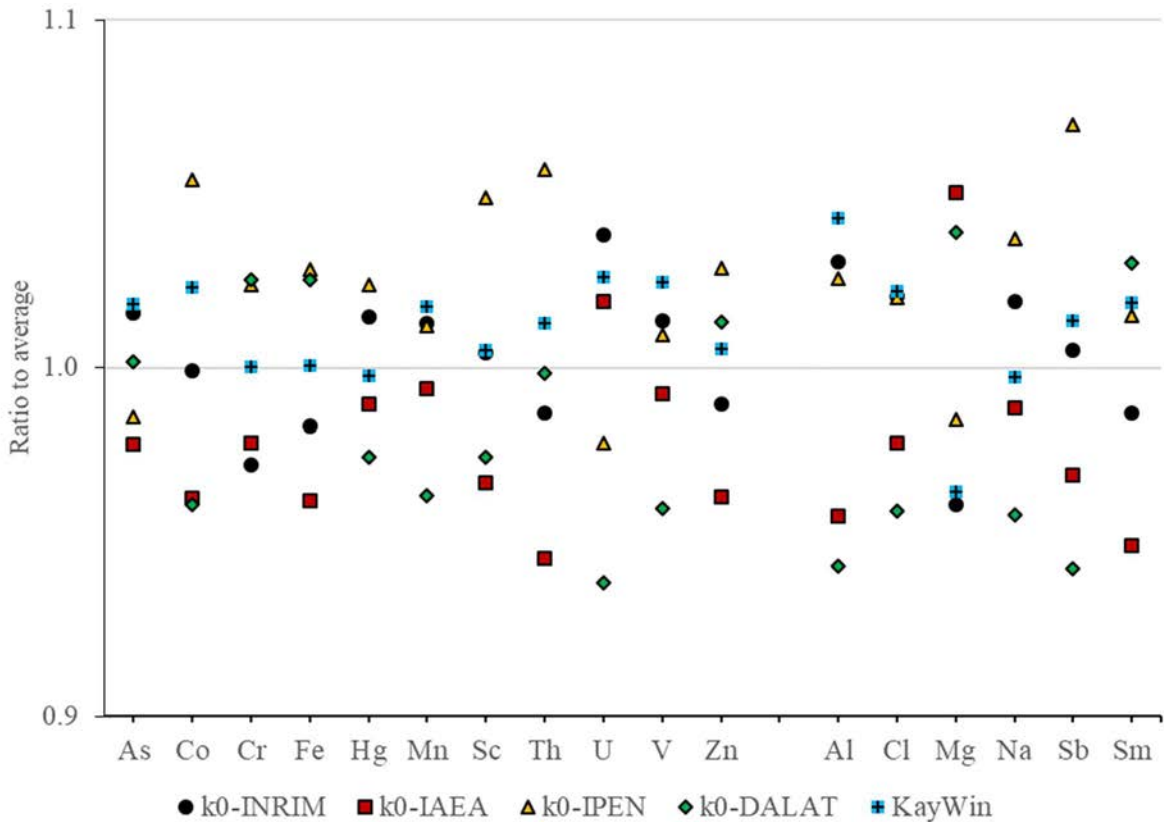


FIG. 31. Ratio between the mass fractions (as reported in the second round) and the average of all codes for that element, after correction for the variation in f and α parameters used. Elements As through Zn were certified, Al through Sm were not.

4.4.3. Efficiency curves

As mentioned above, the efficiency ratios shown in Figures 26–28 are used directly to calculate the mass fractions, which are inversely proportional to the sample to monitor efficiency ratios. The differences between the efficiency ratio determined by the individual codes, necessarily lead to differences between the calculated mass fraction values. When considering one single gamma ray peak, a simple linear inverse relationship between the mass fraction differences and the efficiency ratios is obtained. In cases where more than one peak, either from different gamma lines or from multiple spectra, was used to calculate a mass fraction, as was the case for most participating codes, then the relationship becomes more complex.

The differences in efficiency ratios given in Figures 26–28 leads to expected differences in the mass fractions calculated by the different participants of several %. For instance, the efficiency ratio for the ^{24}Na 2754 keV peak has a 17% dispersion for the measurement at 22 mm from the end cap, which would be propagated to the mass fraction if the 1368 keV peak were absent or had been disregarded.

It can be concluded that the determination of the detector's efficiency curves, and the conversion of these from one counting geometry to another, is a major source of variation in the mass fractions determined by the different codes in the intercomparison done.

4.4.4. Gamma ray interferences

Gamma ray interference corrections were applied by some of the participants in the first round, and by all in the second. They only changed the results significantly for Hg.

4.4.5. Threshold reaction interferences

The codes k0-DALAT, k0-INRIM, k0-IPEN and KayWin do not always apply threshold interference reactions automatically. k0-DALAT needs user input if the flux monitor does not contain nickel. In k0-INRIM and k0-IPEN, the user can input values for the interference corrections, calculated externally to the code by some other method. KayWin includes predetermined correction, which can be applied as user option. k0-IAEA always applies the threshold corrections automatically. The capture cross sections are not standardized in the k_0 library, and each code may use different ones, which contributes to the variation in results for Mg, as well as in the reported values for the fast neutron flux.

5. CONCLUSIONS

An intercomparison exercise of k_0 software packages was organized, with five codes taking part. Of these, two are widely used and three were developed in particular institutions where they are used. Data was collected by a proficient practitioner of a proficient NAA laboratory, using a CRM as sample, and including all the data and information needed for the analysis, including for characterization of the detection system and of the irradiation facility, and distributed to the participants together with a template for reporting. Information on the sample was limited to stating the type of sample (soil/sediment), without any information on which CRM or even the elements that should be reported. The participants were either the code authors or most experienced users from the originating institution.

The first round of reporting of results, which was fully blind, led to an overall standard deviation of reported mass fractions, considering all elements and all codes, of 6.4%. As experimental sources of variation were eliminated from the intercomparison, this is the value that could be taken to correspond to the additional uncertainty due to the code used, for the codes as they were at the beginning of the exercise, when used by knowledgeable users.

However, the fact is that in several cases, and in spite of the participants being all very experienced and proficient practitioners, some important factors were not fully addressed in the first round. This included the k_0 data, which was not always that of the current k_0 database, interference and/or threshold corrections not (or not completely) included in the calculation, detector efficiency values not corrected with respect to the reference position, and inadequate quantification of the fast flux. Moreover, all codes except KayWin improved some part of the calculation.

While some of these factors affected the results provided by a given participant for all the elements reported, others affected particular elements only. So, the 6.4% standard deviation mentioned above is mostly due to two elements, namely Hg and Mg, which suffer most strongly from interferences among the elements used for the intercomparison.

After receiving the results from the first round, and with knowledge of the identity of the CRM and discussion among the group of participants, the codes could be improved and a second round of calculations ensued. As a second factor contributing for improvement, all participants applied the relevant corrections. As a result, the overall standard deviation of reported mass fractions, considering all elements and all codes, decreased from 6.4% in the first round to 3.0% in the second round of reporting. This 3.0% can be taken to correspond to the additional contribution to the k_0 -NAA uncertainty budget due to the code used, for best use of the codes as they were at the end of the intercomparison exercise.

One should note that, even when aware of the special nature of this particular data analysis, best use of the codes was not applied in all cases. This demonstrates that results obtained with a powerful and well understood method such as k_0 -NAA, with an inherent uncertainty of a few percent, can easily have a much larger uncertainty. This has been observed in practice in the IAEA proficiency testing of NAA laboratories by intercomparison exercises [47], in which some k_0 -NAA laboratories consistently obtain extremely good results, while others oscillate in performance, obtaining sometimes poor results.

One should note that the procedure to include interference corrections is not part of the k_0 -NAA method, and each software developer developed their own methodology. In one case the corrections are included in the software and are always applied (k0-IAEA), in one case they are included as user option that the user must select (KayWin), and for the other codes (k0-DALAT,

k_0 -INRIM, k_0 -IPEN), they need to be calculated by other means and input by the user. Threshold reaction interferences rely on fast neutron capture cross sections or other methods that are typically determined in-house for each irradiation facility.

Furthermore, analysis of the results of the intercomparison exercise established that, once analysis errors are eliminated and interferences are adequately taken into account, the main factor that impacted the calculated elemental mass fractions was the detector characterization. This includes the radionuclides and peak energies used for the characterization, as well as the polynomial equations used for the detector efficiency curve. In addition, it was observed that the procedure employed to characterize the irradiation facility (i.e. ‘Cd-cover’ versus ‘triple bare’) also has an impact on the calculated mass fractions.

Different flux monitors and calibration sources can be used for the characterization of the detector and of the irradiation facility. The determination of the k_0 parameters f and α can also be made in different ways. Different participants made different choices, based on their own experience and on the single dataset available. These choices also contributed to the dispersion in mass fractions reported by the different codes, and are included in the final 3.0% standard deviation obtained for all elemental mass fractions.

It is important to note that, for those elements that had certified mass fractions, the mass fractions reported by all codes were in agreement with the certified values, within the uncertainties specified in the CRM certification report, which were between 2.5 and 5.3% for $k=1$ coverage. This demonstrates the validity of the data in the k_0 database, for the elements in question, to within the uncertainties reported.

At the same time, all codes exhibited good statistical control in the sense that reported mass fractions agreed with certified mass fractions to within the specified uncertainties.

Best practices, when applying the k_0 -NAA method, include:

- Careful characterization of the detector, using a large number and wide energy range of gamma ray lines;
- Adequate application of relevant interference and threshold capture corrections, including determination of the fast neutron flux;
- Use of a low-Q activation reaction for flux monitoring, instead of Au, in order to reduce the possible impact of inaccurate f , α determination of the majority of mass fractions that are determined through low-Q reactions;
- Adequate correction of the detector efficiency, when the measurement position is not equal to the reference position used for detector calibration;
- Use of the current k_0 database;
- Inclusion of a reference material and a blank with the samples, in particular when initially implementing the k_0 -NAA method.

Finally, the data, the template for reporting and the results as reported by the participants are given in Annexes 1 to 3, and can assist any future code developers in their efforts, as they provide well characterized and assessed data that can be use for verification of the results provide by the codes.

REFERENCES

- [1] SIMONITS, A., DE CORTE, F., HOSTE, J. Single-comparator methods in reactor neutron activation analysis, *J. Radioanal. Chem.* **24** (1975) 31–46.
- [2] MOENS, L., et al., Calculation of the absolute peak efficiency of gamma-ray detectors for different counting geometries, *Nucl. Instrum. Methods* **187** (1981) 451–472.
- [3] VAN SLUIJS, R., BOSSUS, D.A.W., Optimized data evaluation for k_0 -based NAA. *J. Radioanal. Nucl. Chem.* **239** (1999) 601–603.
- [4] VAN SLUIJS, R., BOSSUS, D.A.W., VERVECKEN, D., KLOK, G., Commercial k_0 -based neutron activation analysis at DSM Research (the Netherlands), *Acta Physica Hungarica* **75** (1994) 355–359.
- [5] BOSSUS, D.A.W., VAN SLUIJS, R., The influence of sample properties and sample geometry on the accuracy of gamma-ray spectrometric analyses, *J. Radioanal. Nucl. Chem.* **233** (1998) 143–148.
- [6] ROSSBACH, M., BLAAUW, M., BACCHI, M., LIN, X., The k_0 -IAEA code, *J. Radioanal. Nucl. Chem.* **274** (2007) 657–662.
- [7] ROSSBACH, M., BLAAUW, M., Progress in the k_0 -IAEA code, *Nucl. Instrum. Methods in Physics Research A* **564** (2006) 698–701
- [8] D’AGOSTINO, G., DI LUZIO, M. ODDONE, M., The k_0 -INRIM software: a tool to compile uncertainty budgets in neutron activation analysis based on k_0 -standardisation, *Measurement Science and Technology* **31** (2020) 017002.
- [9] DI LUZIO, M., D’AGOSTINO, G., The k_0 -INRIM software version 2.0: presentation and an analysis vademecum, *J. Radioanal. Nucl. Chem.* **331** (2022) 4251–4258.
- [10] ROBOUCH, P., ARANA, G., EGUSKIZA, M., Uncertainty Budget for k_0 -NAA, *J. Radioanal. Nucl. Chem.* **245** (2000) 195–197.
- [11] INTERNATIONAL ATOMIC ENERGY AGENCY, Intercomparison of Gamma Ray Analysis Software Packages, IAEA-TECDOC-1011, Vienna (1998).
- [12] BLAAUW, M., OSORIO FERNANDEZ, V., WESTMEIER, W., IAEA γ -ray spectra for testing of spectrum analysis software, *Nucl. Instrum. Methods in Physics Research A* **387** (1997) 410–415.
- [13] BLAAUW, M., et al., The 1995 IAEA intercomparison of commercially available γ -ray spectrum analysis software, *Nucl. Instrum. Methods in Physics Research A* **387** (1997) 416–432.
- [14] GARCÍA-TORAÑO, E., CRESPO, M.T., WOODS, S., BLAAUW, M., FAZINIC, S., The 1997 IAEA Test Spectra for Alpha-particle Spectrometry, *Nucl. Instrum. Methods in Physics Research A* **428** (1999) 330–335.
- [15] BLAAUW, M., GARCÍA-TORAÑO, E., WOODS, S., FAZINIC, S., The 1997 IAEA Intercomparison of Commercially Available PC-based Software for Alpha-Particle Spectrometry, *Nucl. Instrum. Methods in Physics Research A* **428** (1999) 317–329.
- [16] LOS ARCOS, J.M., BLAAUW, M., FAZINIC, S., KOLOTOV, V.P., The 2002 IAEA test spectra for low-level γ -ray spectrometry software, *Nucl. Instrum. Methods in Physics Research A* **536** (2005) 189–195.
- [17] ARNOLD, D., BLAAUW, M., FAZINIC, S., KOLOTOV, V.P., The 2002 IAEA intercomparison of software for low-level γ -ray spectrometry, *Nucl. Instrum. Methods in Physics Research A* **536** (2005) 196–210.
- [18] INTERNATIONAL ATOMIC ENERGY AGENCY, Intercomparison of PIXE spectrometry software packages, IAEA-TECDOC-1342, Vienna (2003).
- [19] BLAAUW, M., et al., The 2000 IAEA intercomparison of PIXE spectrum analysis software, *Nucl. Instrum. Methods in Physics Research B* **189** (2002) 113–122.

- [20] PESSOA BARRADAS, N., et al., International Atomic Energy Agency inter-comparison of Particle Induced Gamma-ray Emission codes for bulk samples, *Nucl. Instrum. Methods in Physics Research B* **468** (2020) 37–47.
- [21] BARRADAS, N.P., et al., International Atomic Energy Agency intercomparison of Ion Beam Analysis software, *Nucl. Instrum. Methods in Physics Research B* **262** (2007) 281–303.
- [22] KUBESOVA, M., KUCERA, J., Comparison of Kayzero for Windows and k_0 -IAEA software packages for k_0 standardization in neutron activation analysis, *Nucl. Instrum. Methods in Physics Research A* **654** (2011) 206–212.
- [23] DE CORTE, F., The k_0 -standardization Method – a move to the optimization of neutron activation analysis, Habilitation thesis, INW, Gent (1987).
- [24] DE CORTE, F., SIMONITS, A., *Vademecum for k_0 -users*, DSM research, Geleen, The Netherlands (1994).
- [25] TRKOV, A., MATSSF Program, <http://www-nds.iaea.org/naa/matssf/>
- [26] ZEROVNIK, G., TRKOV, A., SNOJ, L., Calculations of Effective Sample Mean Chord Length for Anisotropic Neutron Flux, *Proc. International Conference on Nuclear Energy for New Europe, Bled, Slovenia, 14–17 September 2009* (2009) 118.1–118.8.
- [27] INTERNATIONAL ATOMIC ENERGY AGENCY, Nuclear Data Section Neutron Activation Analysis Portal, <https://www-nds.iaea.org/naa/portal.html>
- [28] JOINT COMMITTEE FOR GUIDES IN METROLOGY, Evaluation of measurement data — Guide to the expression of uncertainty in measurement, *JCGM 100:2008* (2010).
- [29] D’AGOSTINO, G., DI LUZIO, M., ODDONE, M., An uncertainty spreadsheet for the k_0 -standardisation method in Neutron Activation Analysis, *J. Radioanal. Nucl. Chem.* **318** (2018) 1261–1269.
- [30] ORTEC AMETEK, GammaVision Gamma Spectroscopy, <https://www.ortec-online.com/products/application-software/gammavision>.
- [31] HYPERLABS SOFTWARE, *HyperLab 2014, Quick start guide for main model*, Budapest, Hungary, (2014).
- [32] DI LUZIO, M., ODDONE, M., D’AGOSTINO, G., Developments of the $k(0)$ -NAA measurement model implemented in k_0 -INRIM software, *J. Radioanal. Nucl. Chem.* **331** (2022) 4251–4258.
- [33] FRANA, J., Program DEIMOS32 for gamma-ray spectra evaluation, *J. Radioanal. Nucl. Chem.* **257** (2003) 583–587.
- [34] VAN SLUIJS, R., et al., Evaluation of three software programs for calculating true coincidence summing correction factor, *J. Radioanal. Nucl. Chem.* **244** (2000) 675–680.
- [35] JOVANOVIĆ, S., DLABAČ, A., MIHALJEVIC, N., VUKOTIC, P., ANGLE: A PC-code for semiconductor detector efficiency calculations, *J. Radioanal. Nucl. Chem.* **218** (1997) 13–20.
- [36] SUDAR, S., “TrueCoinc, a software utility for calculation of the true coincidence correction”, in *IAEA-TECDOC-1275* (2002) 37–48.
- [37] GUNNINK, R., PRINDLE A.L., Nonconventional methods for accurately calibrating germanium detectors, *J. Radioanal. Nucl. Chem.* **160** (1992) 305–314.
- [38] DI LUZIO, M., D’AGOSTINO, G., M. ODDONE, A method to deal with correlations affecting γ -counting efficiencies in analytical chemistry measurements performed by k_0 -NAA, *Measurement Science and Technology* **31** (2020) 074006.
- [39] NATIONAL INSTITUTE OF STANDARDS AND TECHNOLOGY, X-Ray Mass Attenuation Coefficients, NIST Standard Reference Database 126, <https://www.nist.gov/pml/x-ray-mass-attenuation-coefficients>
- [40] BRIESMEISTER J.C. (Ed), *MCNP-A General Monte Carlo N-Particle Transport Code, Version 4C*, Los Alamos National Laboratory Report LA-13709-M, Los Alamos (2000).

- [41] VAN SLUIJS, R., BOSSUS, D., Optimized data evaluation for k0-based NAA, *J. Radioanal. Nucl. Chem.* **239** (1999) 601–603.
- [42] INTERNATIONAL ATOMIC ENERGY AGENCY, Introduction to Quality Management for EDXRF Practice, Training Course Series (CD-ROM) No. 53, Vienna (2012).
- [43] GILMORE, G., *Practical Gamma-ray spectrometry*, 2nd edn, Wiley (2008).
- [44] INTERNATIONAL ATOMIC ENERGY AGENCY, Determination and Interpretation of Characteristic Limits for Radioactivity Measurements, IAEA Analytical Quality in Nuclear Applications Series No. 48, Vienna (2017).
- [45] DI LUZIO, M., K0-INRIM GitHub Repository, <https://github.com/marcodiluzio/k0-INRIM>
- [46] INTERNATIONAL ATOMIC ENERGY AGENCY, Proficiency Testing by Interlaboratory Comparison Performed in 2010–2015 for Neutron Activation Analysis and Other Analytical Techniques, IAEA-TECDOC-1831, Vienna (2017).
- [47] RIDIKAS, D., PESSOA BARRADAS, N., MIGLIORI, A., KATUKHOV, A., BODE, P., Improved Performance of Neutron Activation Analysis Laboratories by Feedback workshops following Interlaboratory Comparison Rounds, *Accreditation and Quality Assurance* **26** (2021) 157–164.
- [48] BUREAU INTERNATIONAL DES POIDS ET MESURES, Monographies — Tables of Radionuclides. <https://www.bipm.org/en/publications/monographies>
- [49] JOINT RESEARCH CENTRE, BCR-320R Channel Sediment (trace elements), <https://crm.jrc.ec.europa.eu/p/40455/40459/By-material-matrix/Soils-sludges-sediment-dust/BCR-320R-CHANNEL-SEDIMENT-trace-elements/BCR-320R>.

ABBREVIATIONS

CRM	Certified reference material
FWHM	Full width at half maximum
GUM	Guide to the expression of uncertainty in measurement
INAA	Instrumental neutron activation analysis
QA/QC	Quality assurance and quality control
k_0 -NAA	Instrumental neutron activation analysis with the k_0 method
NAA	Neutron activation analysis
STD	Standard deviation

CONTENT OF THE ANNEXES

Annex I contains the dataset used for the intercomparison exercise.

Annex II contains the template for reporting.

Annex III contains the results reported for the first and second rounds of intercomparison.

The supplementary electronic files are available on the landing page of this publication at www.iaea.org/publications.

CONTRIBUTORS TO DRAFTING AND REVIEW

D'Agostino, G.	Istituto Nazionale di Ricerca Metrologica, Italy
Blaauw, M.	Delft University of Technology, The Netherlands
Da Silva Dias, M.	Instituto de Pesquisas Energéticas e Nucleares, Brazil
Di Luzio, M.	Istituto Nazionale di Ricerca Metrologica, Italy
Farjallah, N.	International Atomic Energy Agency
Ho-Manh, D.	Center for Nuclear Technologies, Viet Nam
Jaćimović, R.	Jozef Stefan Institute, Slovenia
Pessoa Barradas, N.	International Atomic Energy Agency
Semmler, R.	Instituto de Pesquisas Energéticas e Nucleares, Brazil
van Sluijs, R.	k0-ware, The Netherlands

Online Meetings

1 June, 23 July, 30 September, 30 October 2020
29 January, 4 March, 26 March, 23 April, 21 May, 18 June, 3 September 2021

Consultancy Meeting

Vienna, Austria: 11 October – 13 October 2021



ORDERING LOCALLY

IAEA priced publications may be purchased from the sources listed below or from major local booksellers.

Orders for unpriced publications should be made directly to the IAEA. The contact details are given at the end of this list.

NORTH AMERICA

Bernan / Rowman & Littlefield

15250 NBN Way, Blue Ridge Summit, PA 17214, USA

Telephone: +1 800 462 6420 • Fax: +1 800 338 4550

Email: orders@rowman.com • Web site: www.rowman.com/bernan

REST OF WORLD

Please contact your preferred local supplier, or our lead distributor:

Eurospan Group

Gray's Inn House
127 Clerkenwell Road
London EC1R 5DB
United Kingdom

Trade orders and enquiries:

Telephone: +44 (0)176 760 4972 • Fax: +44 (0)176 760 1640

Email: eurospan@turpin-distribution.com

Individual orders:

www.eurospanbookstore.com/iaea

For further information:

Telephone: +44 (0)207 240 0856 • Fax: +44 (0)207 379 0609

Email: info@eurospangroup.com • Web site: www.eurospangroup.com

Orders for both priced and unpriced publications may be addressed directly to:

Marketing and Sales Unit

International Atomic Energy Agency

Vienna International Centre, PO Box 100, 1400 Vienna, Austria

Telephone: +43 1 2600 22529 or 22530 • Fax: +43 1 26007 22529

Email: sales.publications@iaea.org • Web site: www.iaea.org/publications

**International Atomic Energy Agency
Vienna**